Geophysical Journal International

Geophys. J. Int. (2017) **210,** 671–692
Advance Access publication 2017 May 10
GJI Geodynamics and tectonics

doi: 10.1093/gji/ggx202

Dripping or delamination? A range of mechanisms for removing the lower crust or lithosphere

Adam P. Beall,[1] Louis Moresi[1] and Tim Stern[2]

[1]*School of Earth Sciences, University of Melbourne, Parkville, Victoria* 3010*, Australia. E-mail: abeall@student.unimelb.edu.au*
[2]*Institute of Geophysics, Victoria University of Wellington, P.O. Box* 600*, Wellington, New Zealand*

Accepted 2017 May 9. Received 2017 May 3; in original form 2016 August 22

SUMMARY

Under some conditions, dense parts of the lower crust or mantle lithosphere can become unstable, deform internally and sink into the less dense, underlying asthenosphere. Two end-member mechanisms for this process are delamination and dripping. Numerical calculations are used to compare the time taken for each instability to grow from initiation to the point of rapid descent through the asthenosphere. This growth period is an order of magnitude shorter for delamination than dripping. For delamination, the growth rate varies proportionally to the buoyancy and viscosity of the sinking material, as with dripping. It also depends on the relative thickness (L_c') and viscosity (η_c') of the weak layer which decouples the sinking material from the upper crust, varying proportionally to $L_c'^2/\eta_c'^{\frac{2}{3}}$. As instabilities commonly resemble a mix of dripping and delamination, the analysis of initial instability growth includes a range of mechanisms in-between. Dripping which begins with a large perturbation and low η_c' reproduces many of the characteristic features of delamination, yet its growth timescale is still an order of magnitude slower. Previous diagnostic features of delamination may therefore be ambiguous and if rheology is to be inferred from observed timescales, it is important that delamination and this 'triggered dripping' are distinguished. Transitions from one mechanism or morphology to another, during the initial growth stage, are also examined. 3-D models demonstrate that when η_c' is small, a dripping, planar sheet will only transition into 3-D drips if the initial triggering perturbation is less than a third of the dense material's thickness. This transition occurs more easily at large η_c', so rheological heterogeneity may be responsible for morphological transitions through time. We also calculate the rates at which delamination grows too slowly to outpace cooling of the upwelling asthenosphere, resulting in stalling and switching to dripping. Common lithospheric viscosities and observed timescales indicate that both instability transitions are feasible. Overall, the timescale and persistence of delamination depends on three parameter groups, which characterize the properties of the anomalously dense material, weak lower crustal layer and relative rate of thermal diffusion. These scalings appear to unify the varying results of previous delamination studies.

Key words: Instability analysis; Numerical modelling; Dynamics: gravity and tectonics; Dynamics of lithosphere and mantle; Intra-plate processes.

1 INTRODUCTION

Although continents are generally buoyant enough to resist recycling by mantle convection, anomalously dense eclogitic lower crust can form through prograde metamorphism (Kay & Kay 1993) or partial melting (Lee *et al.* 2006) and dense mantle lithosphere by cooling (Poudjom Djomani *et al.* 2001). If this dense continental material is perturbed and sinks into the mantle (Fig. 1), its evolution is typically thought to evolve by dripping (technically the Rayleigh–Taylor Instability, RTI, Chandrasekhar 1961; Houseman & Molnar 1997) or delamination (Bird 1979). Which mechanism dominates depends firstly on whether prerequisite conditions are met and then on which one can develop more quickly. Delamination requires a weak lower crust and has to be triggered by an external geological process which can effectively displace the lithosphere-asthenosphere interface up to meet the lower crust (Morency & Doin 2004). Dripping also requires a large triggering perturbation or stress-dependent weakening of cold lithosphere, in order to develop more quickly than thermal diffusion can smooth out any perturbation of the lithosphere-asthenosphere interface (Conrad & Molnar 1997; Molnar & Jones 2004). These initial conditions can be present to varying degrees and attributed to a range of

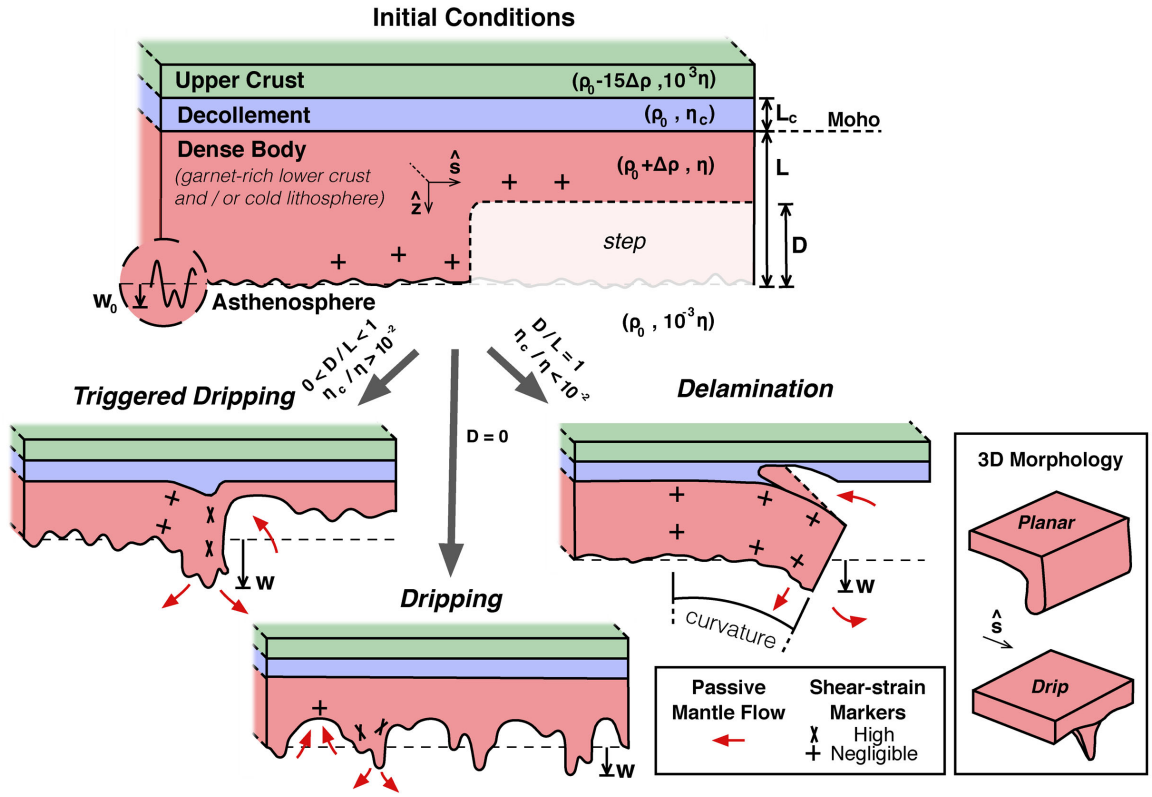

Figure 1. Schematic diagram of the initial conditions and the three mechanisms that can develop depending on these conditions. The primary parameters which are varied are the initial step-size D and the decollement viscosity η_c, while the other parameters are described in Table 1. Density and viscosity are shown in brackets for each material and the parameters are set up so they can be applied to any dense body thickness, density and viscosity. For an initial $D = 0$, the subsequent flow follows the Rayleigh–Taylor Instability (RTI) model and is referred to as the dripping mechanism. Its flow is characterized by high internal shearing and even though the Moho may be displaced, the top of the dense body remains connected to the decollement layer. Delamination can be triggered when $D = L$, so that the asthenosphere is adjacent to the decollement, which also needs to be weak enough that it can subsequently flow and allow the dense body to peel away. Delamination occurs with negligible shear-strain of the dense body. If $D > 0$, as may be the case if tectonic strain produces a large perturbation as suggested by Stern *et al.* (2013), the instability still grows primarily by thickening, with non-negligible shear-strain, but may have an appearance similar to delamination. This hybrid mechanism is referred to as 'triggered dripping'. In 3-D models (inset), the morphology of the sinking material is characterized as either a 'drip', which has a circular shape in horizontal cross-section, or being 'planar', in which the sinking material is sheet-like.

instabilities globally, as described in the following discussion, leading to the appearance of a range of instabilities between the dripping and delamination end-members. Numerical models are used in this study to demonstrate that there are three discrete instability mechanisms (Fig. 1) which are triggered by specific conditions and evolve with significantly contrasting dynamics.

Dripping instabilities which grow from a small amplitude perturbation (Chandrasekhar 1961) have been proposed to explain the evolution of sinking lithosphere beneath the Carpathians (Lorinczi & Houseman 2009) and the switch from shortening to extension observed in Tibet and the Basin and Range, USA, amongst other examples (Houseman & Molnar 1997). Stress-dependent weakening is important in such models, as the instability timescale predicted using the relatively high viscosity of cold mantle lithosphere or lower crustal eclogite, is much slower than typically observed. Even with such weakening, dripping from a small perturbation typically occurs too slowly to reproduce observed timescales (Molnar & Jones 2004).

Dripping triggered by a large amplitude perturbation (Canright & Morris 1993), hereafter abbreviated to 'triggered dripping', can reproduce the rapid <10 Ma removal timescale of the sinking lower crust and mantle lithosphere beneath the Sierra Nevada, USA, assuming that the eastern edge of the dense material had been thinned locally by 50 per cent and separated from the strong upper crust by a weak layer (Molnar & Jones 2004). The instability timescale is slower by at least an order of magnitude in the absence of either of these two criteria. Molnar & Jones (2004) subsequently suggested that the dense material was effectively stable, until a zone of localized strain migrated from the Basin and Range region (detailed by Jones *et al.* 2004) and triggered the rapid instability.

Dripping may also have been triggered by large amplitude perturbation of the cold lithosphere beneath the North Island, New Zealand (Stern *et al.* 2013). The mantle lithosphere is inferred to have effectively thinned by 85 per cent, as a result of strike-slip offset, generated by subduction zone migration over the last 5 Ma (detailed by Lamb 2011). A weak lower crust was proposed to explain the significant southward migration of the instability. Such a weak layer is a requirement for delamination (Bird 1979) and at high displacement the mantle lithosphere is modelled by Stern *et al.* (2013) as peeling away from the crust. If only the peeled state is observed, it would be difficult to discern whether the instability had been triggered by thinning of the mantle lithosphere of 85 per cent or 100 per cent, the latter required for delamination. It is therefore unclear whether there is a significant difference in the mechanisms of instabilities beginning with the conditions for triggered dripping and delamination.

Delamination can be triggered in models when the dense lower crust and/or mantle lithosphere layer is thinned by 100 per cent.

Some models of the Sierra Nevada instability involve thinning of the mechanical lithosphere by 100 per cent, invoked as an imposed weak region resulting from subduction-related hydration (Valera *et al.* 2014) or dynamic plastic weakening related to the localization of the previously discussed Basin and Range deformation (Le Pourhiet *et al.* 2006). In active subduction zones, such as beneath the Andes and previously beneath Tibet, a mixture of eclogitic lower crust and cold mantle lithosphere is inferred to have delaminated when significant effective thinning was triggered by slab roll-back (Sobolev & Babeyko 2005) or when weak eclogite sunk through the mantle lithosphere and generated a weak channel (Krystopowicz & Currie 2013).

1.1 Range of mechanisms and corresponding growth rates

The identification of dripping, triggered dripping and delamination instabilities combine to give a complete mechanism map, which depends on the lower crustal strength and initial perturbation size. Morency & Doin (2004), Göğüş & Pysklywec (2008) and Krystopowicz & Currie (2013) describe specific lower crustal viscosity thresholds, above which delamination does not initiate and the instability takes considerably longer to grow. This discrete behaviour may occur due to the use of plasticity. The triggered dripping models of Stern *et al.* (2013) do not include plasticity and the weak lower crust is imposed. These models begin with the conditions for triggered dripping, but evolve in a way which qualitatively resembles delamination, potentially indicating that the mechanics and dynamics of delamination are not significantly different to triggered dripping. This is difficult to test quantitatively, because there is no general framework for quantifying how long it takes for a dense layer with a given thickness, density and viscosity, to thicken by a significant amount, depending on whether triggered dripping or delamination occur.

The sinking velocity increases through time for dripping, triggered dripping and delamination (Canright & Morris 1993; Houseman & Molnar 1997; Bajolet *et al.* 2012), so the characteristic growth timescale is a measure of acceleration. In linear stability analysis this is called the growth rate, τ (Chandrasekhar 1961). The instability growth rate is well understood for the dripping end-member and can be easily calculated from existing models by scaling non-dimensional growth rates by the properties of any given dense material (Houseman & Molnar 1997). There is no equivalent simple calculation of the delamination growth rate, though previous studies have shown which parameters it is likely to depend on. Bird & Baumgardner (1981) and Bajolet *et al.* (2012) have shown that the delamination growth time is influenced by the rheology and thicknesses of the lower crust, though there is no mathematical model or scaling describing this dependence. The delamination timescale also appears to vary, potentially linearly, with the density and viscosity of the unstable material (Bajolet *et al.* 2012; Krystopowicz & Currie 2013; Wang & Currie 2015). Alternatively, Le Pourhiet *et al.* (2006) argue that the rheology of the asthenosphere, rather than lithosphere, predominately controls the sinking velocity of delaminating material. The conditions for the initiation of delamination also depend on many parameters, including the largest initial density anomaly (Krystopowicz & Currie 2013) and plastic strength of the lithosphere (Morency & Doin 2004), though the processes leading to mechanism initiation are not considered in this study.

The growth rates of the instabilities varying between the dripping and delamination end-members could be used to predict which instability mechanism is most effective for recycling dense subcontinental material on Earth. This prediction cannot be clearly made by comparing previous studies. In the models of Göğüş & Pysklywec (2008), delamination ('DEL') takes 1.2 Ma to displace the lithosphere by about 230 km and is approximately 10 $\times$ faster than dripping beginning with a significant perturbation ('DRIP-1'). This rapid <5 Ma timescale is shared by other delamination models, such as 'Model 2' in Krystopowicz & Currie (2013), 'Simulation 6' in Morency & Doin (2004) and 'Delamination 2' in Wang & Currie (2015). The rapid recycling occurs in these models occurs only after the conditions for delamination are dynamically generated, which can take <40 Ma. The triggered dripping mechanism can also grow to a significant vertical displacement within $\sim$5 Ma, for stress-dependent rheology (Molnar & Jones 2004). As in Göğüş & Pysklywec (2008), Wang & Currie (2015) calculated a comparative dripping model, beginning from a small amplitude perturbation, but sinking occurs as quickly as for delamination.

Overall, it is unclear if dense material would always sink more quickly if delamination is triggered, compared to dripping with various initial perturbations. The difficulty in making this comparison is most likely due to contrasts in rheological assumptions, density profiles and initial conditions, between the different studies. In this study, scaling laws and non-dimensional growth rates are measured from numerical models which are simplified for this purpose. In doing so, the initial evolution of delamination is directly compared to the analytical dripping model, which also applies to triggered dripping, so that the fundamental timescales of the three mechanisms can be described in an equivalent manner.

1.2 Delamination definition

Delamination is typically defined as being any mechanism which involves the separation of the dense layer from the crust as it sinks. This definition does not prescribe how the sinking body should be deformed internally, for example if it thickens, or what physical process results in its increasing velocity. We assume a more precise definition of delamination, by assuming a delaminating body deforms by viscous bending, as in Bird (1979). If it is assumed that the dense layer bends with uniform curvature (Fig. 1), then it deforms by pure bending, for which it should peel away with negligible internal shear-strain. Most existing models of delamination appear to approximately meet this definition during the initial peeling of the dense layer from the crust (Morency & Doin 2004; Göğüş & Pysklywec 2008; Bajolet *et al.* 2012; Gray & Pysklywec 2012; Wang & Currie 2015).

The models of Stern *et al.* (2013) reproduce some characteristics of delamination: the migration of asymmetric topography (Göğüş & Pysklywec 2008; Wang & Currie 2015) and the peeling away from a low viscosity lower crust (Bird & Baumgardner 1981; Morency & Doin 2004). The lithosphere however, undergoes significant shear-strain as it sinks. A similar deformation style has been inferred seismologically for the sinking material beneath the Colorado Plateau (Levander *et al.* 2011), where the lithosphere appears to have peeled away from the lower crust by $\sim$40 km, but through internal strain the base of the lithosphere has been displaced to a depth of 250 km. Such instabilities deform in a different way to our specific definition of delamination and their sinking velocity evolution may therefore also differ, as is argued in this study. The definition of the delamination mechanism as occurring with negligible shear-strain is an important aspect of this analysis, as it will be shown that instabilities such as modelled by Stern *et al.* (2013), which share the

characteristics of delamination without satisfying our definition, actually follow the analytic dripping growth models instead.

1.3 Temperature-dependent instability transitions

Given the specific conditions required to initiate delamination, it is plausible that a change in these conditions could force an instability to switch from delamination to dripping. The required low viscosity decollement zone could plausibly increase in viscosity through time due to cooling. Valera *et al.* (2014) observed that after 5 Ma, the asthenosphere flowing into the lower crust above the peeling mantle lithosphere cooled down, increasing the viscosity of this region. There may plausibly be relative thermal diffusion timescales at which this is likely to happen and could explain the mixture of peeling and lithospheric thickening which appears to have occurred below the western Colorado Plateau (Levander *et al.* 2011). 2-D thermal models are used to calculate how slowly delamination must evolve for significant cooling to occur, as well as to test whether this instability switch can occur.

Additionally, a switch in '3-D morphology' (Fig. 1, inset) could occur during instability growth. The preferential morphology of dripping is the localized 'drip morphology', though if the lithosphere is significantly perturbed with an initial planar displacement, it could grow with a 'planar morphology' (Ribe 1998; Kaus & Podladchikov 2001). Delamination is typically modelled as a 2-D process, peeling in only one direction with a 'planar morphology'. There is the possibility that 2-D modelling is biased towards delamination and that some modelled instabilities in 3-D would switch to 3-D drips. With the increasing influence of thermal diffusion, it is also possible that small wavelength drips could be thermally erased more quickly than large wavelength 2-D perturbations. We investigate whether this morphology switch is likely to occur and how it may be affected by the weak lower crust and large lithospheric perturbation required for delamination to occur.

Such a morphology transition may have occurred during the evolution of the sinking dense lower crust beneath the Sierra Nevada, USA. The dense body appears to have originally extended ~450 km along strike of the batholith, whereas the current extent observed in tomography is ~100 km (Frassetto *et al.* 2011; Gilbert *et al.* 2012; Jones *et al.* 2014). As the dense lower crust extent has not changed considerably perpendicular to the batholith strike, this is a transition from a planar to a drip morphology. The initial large perturbation on the eastern side of the dense body (Molnar & Jones 2004; Valera *et al.* 2014) if it extended along the entire 450 km extent, as well as a weak lower crust, are likely to make the transition to a drip morphology more difficult. The conditions for such a transition to occur are tested using the temperature-dependent 3-D numerical models.

1.4 Rayleigh–Taylor instability theory

The velocity of dripping material through time has long been described by the RTI model (Chandrasekhar 1961; Turcotte & Schubert 2014). It consists of two layers of fluid, in this case the dense lower crustal and/or lithospheric layer and the asthenosphere of lower density below (Fig. 1), separated by a horizontal interface which is perturbed by a displacement w. The initial value of w, denoted w_0, is generally assumed to small compared to the thickness of the dense layer. This configuration is unconditionally unstable and its initial evolution is greatly simplified using the 'small displacement' assumption: that the growing perturbation displacement is small compared to the dense layer thickness. In this case the perturbation grows exponentially with a growth rate τ (eq. 1, symbols in Table 1). τ can be separated into a buoyancy flow timescale, $\Delta\rho g L/\eta$ and a non-dimensional part, τ', which depends on boundary conditions, the rheology of the crust and asthenosphere, as well as a range of other problem-specific parameters. The buoyancy flow timescale depends on the difference by which the dense layer is denser than the underlying asthenosphere ($\Delta\rho$), the gravitational acceleration (g), the dense layer thickness (L) and the viscosity of the dense layer (η):

$$w = w_0 e^{\tau(\lambda)t}$$
$$\tau = \frac{\Delta\rho g L}{\eta}\tau'(\lambda). \quad (1)$$

The small displacement RTI solution is typically simplified using Fourier decomposition (Chandrasekhar 1961), expressing the perturbation as the summation of waveforms, each with a wavelength λ and its own τ'. Because w grows exponentially through time, the velocity field can be well approximated by the term in this sum with the highest growth rate. The general approach in analytical modelling (e.g. Chandrasekhar 1961; Houseman & Molnar 1997; Conrad & Molnar 1999) is then to solve the dependence of τ' on λ, taking the maximum τ and the corresponding λ. The small displacement instability growth is then described by the simple expression eq. (1), using these values of τ' and λ, as well as the buoyancy flow timescale. $\tau'(k)$ has been calculated analytically for a range of density and viscosity profiles, non-linear rheologies and multiple layers (Conrad & Molnar 1999; Houseman & Molnar 1997; Neil & Houseman 1999), all demonstrating good agreement with the early growth in numerical calculations.

As eq. (1) is only valid for small displacements of w, Canright & Morris (1993) developed analytic non-linear models, for cases in which the sinking body is much more viscous than the asthenosphere and has a free-slip boundary condition at its top surface. At high w, instabilities approximately grow according to a hyperbolic function of time (eq. 2), which agrees with numerical calculations (Neil & Houseman 1999). Eq. (2) has been expressed here using the same variables and non-dimensionalization of time as introduced for the small displacement analysis. The super-exponential growth rate then again depends on the buoyancy flow timescale and a non-dimensional growth rate τ_2'. In the models of Canright & Morris (1993), $\tau_2' = 0.125$. However, it varies from this in cases where the assumption of a free-slip dense layer surface is no longer valid, but large w growth still follows a hyperbolic relationship (Neil & Houseman 1999). The displacement rapidly approaches infinity as t approaches the singularity in eq. (1) at $t = (\tau_2(w_0 + L))^{-1}$, at which point either the drip breaks off or forms a vertical channel. Using steady subduction as an analogue, flow in a vertical channel is likely to occur at a constant 'Stokes creeping flow' velocity (Capitanio *et al.* 2007). Instability growth in Canright & Morris' (1993) model occurs through localized thickening of the dense body and is therefore not necessarily applicable to peeling instabilities where this is negligible.

$$w = \left(\frac{1}{w_0 + L} - \frac{\tau_2\, t}{L}\right)^{-1} - L$$
$$\tau_2 = \frac{\Delta\rho g L}{\eta}\tau_2' \quad (2)$$

Two or three analytic models can then be used to represent the complete growth of a RTI (Fig. 2): first it follows the 'small displacement' exponential growth at growth rate τ, then super-exponential

Table 1. Commonly used symbols.

Symbol	Meaning	Non-dimensionalization
w	Displacement of the dense body-asthenosphere interface perturbation	$w' = w/L$
w_m	Displacement of the dense body-crust interface (the Moho)	$w'_m = w_m/w$
$\dot{w}$	Interface perturbation velocity (vertical component)	$\dot{w}' = \dot{w}\ \eta/(\Delta\rho g L^2)$
t	Time elapsed since triggering	$t' = t\,\Delta\rho g L/\eta$
w_0, $\dot{w}_0$	Values of w and $\dot{w}$ at $t = 0$	
D	Initial step perturbation size	$D' = D/L$
η_c	Decollement viscosity	$\eta'_c = \eta_c/\eta$
η	Dense body viscosity	–
L	Dense body thickness	–
L_c	Decollement thickness	$L'_c = L_c/L$
$\Delta\rho$	Density contrast between the dense body and asthenosphere	–
ΔP	Pressure anomaly at the decollement edge (not an independent variable)	–
ρ_0	Asthenospheric density	–
g	Gravitational acceleration	–
τ	Initial exponential growth rate	$\tau' = \tau\ \eta/(\Delta\rho g L)$
τ_2	Secondary non-linear growth rate	$\tau'_2 = \tau_2\ \eta/(\Delta\rho g L)$
σ_s	Isostatic compensation stress	$\sigma'_s = \sigma_s/(\Delta\rho g L)$
$\hat{z}$, $\hat{s}$	Vectors pointing down and perpendicular to step	–
λ, $\lambda_{\max}$	Perturbation wavelength: individual or specifically the fastest growing	–
	Temperature-dependent model parameters	
Ra_δ, Ra	Boundary layer and mantle convection Rayleigh Numbers	–
T, ΔT	Temperature field and the mantle potential temperature	$T' = T/\Delta T$
κ	Thermal diffusivity	–
α	Coefficient of thermal expansion	–
β	Arbitrary viscosity scaling coefficient	–

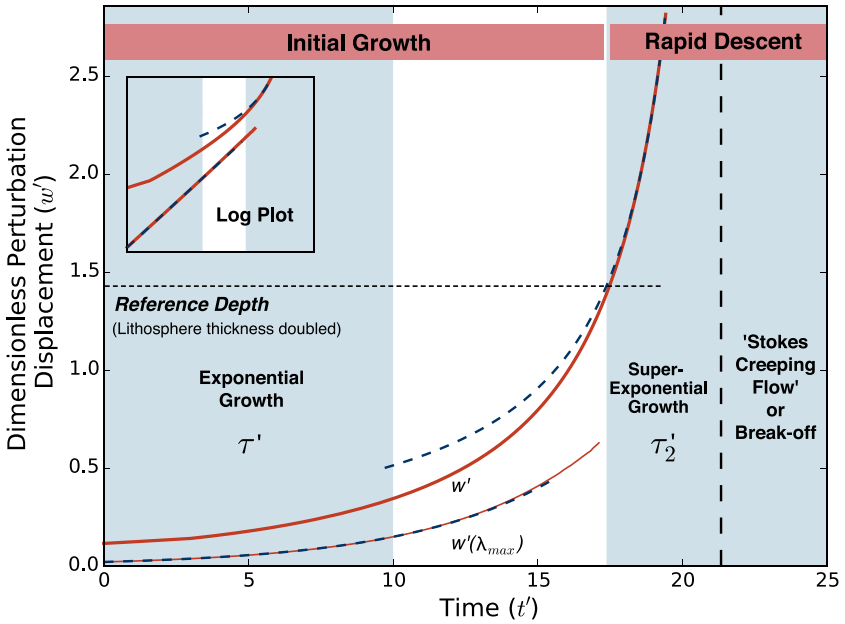

Figure 2. Typical non-dimensionalized perturbation displacement (w') over dimensionless time (t') for the RTI (thick, red solid line), $D' = 0$ and $\eta'_c = 1$. The analysis includes both the total displacement w' and the individual contribution from the fastest growing wavelength $w'(\lambda_{\max})$. The latter is only important when $D' = 0$. Blue dashed lines denote the fitted analytic models of τ and τ_2 from eqs (1) and (2). We only analyse the initial exponential growth and beginning of the following super-exponential growth, though flow will eventually reach a constant velocity, probably characterized as 'Stokes creeping flow' (Capitanio *et al.* 2007) or the drip will break off.

growth with growth rate τ_2, after which the drip breaks off or forms a sheet with a constant velocity. The initial exponential growth phase ('initial growth', Fig. 2) is the primary focus of this study, because it is the slowest phase in the instability evolution and controls the time taken for a typically insignificant w_0 to grow to a prominent displacement. When the instability reaches the super-exponential growth phase, its velocity has typically grown by an order of magnitude and its transit through the upper mantle occurs relatively quickly ('rapid descent', Fig. 2). As the increasing velocity of a delaminating body is likely to occur by a different mechanism to

dripping, delamination may not necessarily be characterized using eqs (1) and (2). However, the two part analytical model (Fig. 2) is used as a reference, so that the relative evolution of RTIs and delamination can be quantified.

1.5 Delamination theory

The fundamental mechanism which allows material to delaminate has not been studied to the same detail as the RTI. Bird (1979) developed an analytic model for predicting the initial sinking velocity ($\dot{w}$) of delaminating lithosphere at small displacement (eq. 3). It assumes that the asthenosphere has intruded up into the lithosphere and into a weak middle to lower crustal layer, referred to as the decollement (Fig. 1). In his model, the relatively buoyant asthenosphere produces a pressure anomaly at the decollement edge (ΔP), which generates horizontal decollement flow and triggers delamination. The deforming decollement is modelled as Poiseuille flow, for which the pressure anomaly linearly decreases in the decollement away from the dense body edge. This pressure gradient in the decollement is coupled to the resisting viscous bending stress of the dense body below, as it peels away. By combining the Poiseuille flow and viscous bending models, Bird calculated the initial vertical velocity for delamination (eq. 3). This analytic theory depends on additional parameters to the RTI: the thickness (L_c) and viscosity (η_c) of the decollement. ΔP is also not necessarily the same magnitude as the pressure anomaly driving the RTI, depending on the model formulation:

$$\dot{w} = \frac{\Delta P L_c}{6^{\frac{1}{3}} L \eta^{\frac{1}{3}} \eta_c^{\frac{2}{3}}}. \tag{3}$$

The delamination velocity in analogue models increases with time (Bajolet *et al.* 2012). Bird & Baumgardner (1981) modelled delamination at high displacement using a combination of analytical and numerical techniques. Their calculated delamination velocity is proportional to the stress load at the edge of the body and therefore the amount of material already delaminated. They reasoned then that its growth should be exponential through time, though this hasn't been tested. Analogue materials engineering models (McEwan & Taylor 1966) have produced a similar relationship between peeling velocity and applied stress.

The delamination model (eq. 3) assumes that the initial gravitational energy is dissipated only through decollement flow and dense body bending. As was previously a point of contention in the subduction literature (Capitanio *et al.* 2007), there remains the possibility that passive mantle flow could play a significant role in dissipating energy. Le Pourhiet *et al.* (2006) argue that delamination is limited primarily by asthenospheric flow. While this may be true for a delaminating body when it has completely peeled away, it has been unclear if the lithospheric viscosity η limits the initial growth up to this point, as it does for the initial velocity in eq. (3).

2 METHODOLOGY

Our primary objective is to compare the initial instability growth timescales of the dripping, triggered dripping and delamination mechanisms. Making this comparison involves first quantifying which mechanism is triggered by a given amount of initial lithospheric thinning and given decollement strength (D and η_c, Fig. 1). The relative timescales are then compared using equivalent measurements of instability growth for each. We aim to make this analysis generalized, so that the dynamic consequences of triggering a particular mechanism can be assessed for any region with dense lower crust and/or mantle lithosphere.

The primary analysis uses a set of 2-D numerical models, described here. They solve the Stokes equation and ignore thermal diffusion. A secondary part of the analysis uses 2-D and 3-D temperature-dependent models to address thermal diffusion effects, which are described later. The initial conditions (Fig. 1) assume the triggering of a particular mechanism *a priori*, so that the focus of the analysis is the initial growing period which immediately follows. Whether dripping, triggered dripping or delamination occurs is controlled by two parameters, D and η_c. D is the size of a large, step perturbation, which is superimposed upon the smaller, random perturbations. It represents a change in the material's thickness which may have been generated by previous deformation, such as strike-slip faulting (Stern *et al.* 2013) or thinning due to plastic failure (Morency & Doin 2004). η_c has been introduced and controls the strength of the middle to lower crust, where a low value reproduces the jelly-sandwich rheological profile (Burov *et al.* 2006). Delamination is generally provoked when $D = L$ and η_c is smaller than η by a couple of orders of magnitude. We define triggered dripping as occurring when $D > 0$, provided delamination does not occur. D and η_c are generally the only two parameters which are varied, so that the gravitational potential energy and the viscosity of the sinking body are constant.

Anomalously high density rocks ($\Delta\rho > 0$) could form in the lower crust or mantle lithosphere in a number of ways. Eclogite can form in the lower crust, with a density 100–600 kg m^{-3} higher than the asthenosphere, as a restitic by-product of crustal melting (Lee *et al.* 2006) or through prograde metamorphism of crustal mafic rocks during orogenesis-related burial (Krystopowicz & Currie 2013). Additionally, though mantle lithosphere is typically 30–75 kg m^{-3} less dense than the asthenosphere when it forms, its density increases to 30–50 kg m^{-3} higher than the asthenosphere once it has cooled to a steady-state geotherm (Poudjom Djomani *et al.* 2001, fig. 4 therein). The iron-depletion of mantle lithosphere is typically greater with age, such that the density contrast $\Delta\rho$ between Proterozoic lithosphere and the asthenosphere is approximately 30 per cent smaller than for Phanerozoic lithosphere. Archean lithosphere generally remains less dense than the asthenosphere, even with a cold geotherm.

Though unstable materials can have a range of densities and thicknesses, all models are non-dimensionalized and therefore can be applied to any of the described dense materials. It is assumed that the unstable material, which could be dense lower crust and/or mantle lithosphere, can be represented as a single material referred to as the 'dense body', with a homogeneous density greater than the asthenosphere by $\Delta\rho$ and thickness L. All quantities are expressed as being proportional to either the buoyancy flow timescale $\Delta\rho g L / \eta$ or the distance L (non-dimensionalization) and so the results can be applied to any dense body using a simple post-processing calculation (dimensionalization). The simplistic dense body formulation should be only cautiously applied to situations in which the sinking material is separated from the asthenosphere or decollement layer by a material which cannot be incorporated into the dense body average, for example, dense lower crust sinking through strong and buoyant mantle lithosphere. Unlike, for example, the models of Krystopowicz & Currie (2013), there are no dynamic densification processes included in this approach. $\Delta\rho$ therefore represents the density of the dense body after eclogite has formed in the lower crust or the mantle lithosphere has cooled.

The majority of models are 2-D and assume that temperature diffusion is negligible on the instability timescale. Each material

has a constant and homogeneous density, which is set relative to the asthenosphere's density (ρ_0) and the anomalous density contrast driving instability ($\Delta\rho$). The dense body has a density of $\rho_0 + \Delta\rho$. The upper crust has a density of $\rho_0 - 15\Delta\rho$. For $\rho_0 = 3300\,\mathrm{kg\,m^{-3}}$ and $\Delta\rho \geq 30\,\mathrm{kg\,m^{-3}}$, this results in a crust which is $<2850\,\mathrm{kg\,m^{-3}}$ and strongly resists sinking. The decollement material is set to a neutral buoyancy, with a density of ρ_0.

Model geometry is defined relative to the dense body thickness L. Generally, the upper crust and decollement layers have equal thicknesses and together form 30 per cent of the total lithosphere thickness, so that each has a thickness of approximately $0.21L$. Though the decollement thickness (L_c) is an important parameter for delamination, it is generally held constant at $L_c = 0.21L$ in order to focus on the effect of varying η_c instead, though it is varied briefly in order to test scaling laws. The total model domain height is set to 6 × the total lithosphere thickness, equivalent to $8.57L$.

The starting small amplitude perturbation (w_0) is set as a cosine series of five random wavelengths, chosen from a set of integer number of waves in the model domain. These wavelengths can range from $0.73L$ to $25.71L$. This range includes wavelengths with the maximum growth rate for analytic models, including with a weak crust or free surface (Houseman & Molnar 1997; Neil & Houseman 1999). The total perturbation amplitude is approximately $0.1L$. Higher resolution RTI models with perturbations with smaller amplitudes and delamination models with no small amplitude perturbations have been tested and the results are unaffected. The random wavelength selection can miss the fastest growing wavelength. This is important for $D = 0$ and for calculating the instantaneous velocity at w_0, so these models are repeated multiple times with different wavelength collections and the highest τ is used. It is ensured that at least some of these include the fastest growing wavelength, calculated from an analytic RTI solution with equivalent layer thicknesses and η_c', as described later.

A Newtonian rheology is used for all models, as the primary focus is the comparison of the simplest delamination instability and RTI cases. Each material has a homogeneous viscosity. For the dense body, this assumes that any stress-dependence or internal layering can be encapsulated by an average η. For the RTI, a stress-dependent viscosity with an exponent of three approximately doubles the maximum growth rate, but does not affect the corresponding wavelength (Conrad & Molnar 1997). Stress-dependence would therefore effectively halve η in eq. (1). In the models, delamination is driven by the same buoyancy stress as dripping, so stress-dependence will likely play an equal or greater role, depending on the magnitude of bending stresses. Additionally, lithospheric stresses generated at high displacement (w) can potentially cause lithospheric necking and break-off, if the lithosphere is modelled with a finite yield strength (Morency & Doin 2004; Krystopowicz & Currie 2013). The Newtonian rheology in our models does not allow this break-off to occur. Our delamination growth timescales are therefore conservative.

The model domain edges all use the free-slip boundary condition (BC). This is equivalent to assuming that all stresses at the domain top are balanced by topography, that the model base corresponds to a substantial viscosity increase at the 660 km mantle discontinuity and that flow is symmetrical at the walls. Though the ceiling BC is set as free-slip, the decollement and dense body essentially have a no-slip ceiling, as the upper crustal material has a viscosity of three and six orders of magnitude higher than the dense body and asthenosphere respectively. The upper crustal layer represents a strong intra-plate crust and is set to a constant thickness of $0.21L$.

The finite-element Lagrangian particle-in-cell code Underworld is used to solve the Stokes equation, assuming incompressibility and plane-strain (Moresi *et al.* 2007). The code has been benchmarked for the RTI (Moresi *et al.* 2001). A Cartesian mesh is used with model domain length:height ratios of 3:1 and a uniformly spaced element resolution of 1296 × 432, as required to accurately measure $w'(\lambda_{\max})$. Each element is populated with at least 20 particles. The model domain depth represents the upper mantle and is six times the thickness of the whole lithosphere.

Parameter non-dimensionalization is described in Table 1 and denoted by a primed variable (t', τ', etc.). Time is always scaled using the buoyancy to viscous stress ratio which arises in the analytic model. Application of this scaling to delamination assumes that flow is generated by the negative buoyancy of the dense body compared to the asthenosphere and the dominant resisting viscosity also belongs to the dense body. The latter would not be the case if energy is primarily dissipated in the asthenosphere, which is ruled out below. Scaling of the decollement parameters are relative to the dense body, as delamination depends on the interplay between dense body and decollement flow.

2.1 2-D and 3-D temperature-dependent models

A secondary objective of this work is to quantify the conditions required for thermal diffusion to influence instability growth. 2-D models are designed to explore whether delamination can be prohibited by cooling of the initially thinned lithosphere. 3-D models are designed to quantify the amplitude of an initially planar perturbation required to prevent 3-D drips from growing (Fig. 1, '3-D Morphology'), particularly as a function of decollement strength and relative thermal diffusion.

A second set of models is required to address these objectives, as the primary set of models is temperature-independent. These secondary models solve for temperature diffusion and may be 2-D or 3-D, coupling the thermal advection-diffusion equation to the Stokes equations (Moresi *et al.* 2007). They are designed identically to the primary set of models, except where noted. The temperature-dependence in Underworld has been extensively benchmarked for thermal convection (Moresi & Solomatov 1995). The temperature-dependent 2-D models use a coarser resolution of 384 × 128, due to the higher computation cost of the coupled equations and the calculation of more time-steps in order to study the instabilities at high amplitude and with thermal convection. The 3-D models use height:length:width ratios of 1:3:2 and a coarser resolution of 128 × 288 × 192. The 3-D mesh is also uniformly spaced and each element is populated with at least 20 particles. These temperature-dependent models begin with an arbitrary temperature (T) field. The surface temperature is maintained as zero and the entire asthenosphere is set to a homogeneous value, ΔT. ΔT is the 'potential mantle temperature' and is the temperature of the mantle if it is adiabatically transported to the surface. The base of the model domain is maintained as ΔT, to prevent any upwellings. The model walls are set as insulating. The Moho is set to $0.5\Delta T$, while separate crust and dense body linear geotherms are set to ensure the temperature field is continuous. As all temperatures are relative to ΔT, T is non-dimensionalized as: $T' = T/\Delta T$.

Only the density and viscosity of the dense body and asthenosphere differ from the primary (temperature-independent) models. The density of both the dense body and asthenosphere is set according to: $\rho_0(1 - \alpha(T - \Delta T))$, where ρ_0 is the material density at $T = \Delta T$ and α is the coefficient of thermal expansion. ρ_0 is identical for the dense body and asthenosphere, so that the density

varies continuously across the asthenosphere-dense body interface. α is set for the dense body such that its average density is $\rho_0 + \Delta\rho$. In the asthenosphere, α is chosen so as to set the thermal convection Rayleigh number, defined as $Ra = \alpha\Delta T\rho_0 g L^3/(10^{-3}\eta\kappa)$, to 10^8, ensuring vigorous convection. κ is the thermal diffusivity and is homogeneous across the model domain and $10^{-3}\eta$ the asthenospheric viscosity at ΔT. The models are intended to be applicable to a range of dimensionalized growth rates, rather than for example a particular κ or $\Delta\rho$, so the ratio of instability flow timescale to thermal diffusion timescale is varied. This relative timescale only depends on the boundary layer Rayleigh number, defined in eq. (4) and varied from $Ra_\delta = 2.79$ to 10^3:

$$Ra_\delta = \frac{\Delta\rho g L^3}{\eta\kappa}. \tag{4}$$

Temperature-dependent viscosity varies according to an arbitrary exponential law: $\mu\beta e^{E'/(T'+T'_0)}$. E' is the activation energy, after it has been non-dimensionalized by ΔT and the gas constant. It is a constant set to $E' = 13.82$, which results in a maximum viscosity contrast of 10^8. T'_0 is an arbitrary non-dimensional temperature which offsets the non-dimensional temperature T', used for example in mantle convection modelling (Lenardic & Kaula 1996), to avoid the extreme viscosity variations at low temperatures which arise for $T'_0 = 0$. It is a constant set to $T'_0 = 0.5$. β is an arbitrary scaling coefficient, where $\beta = 10^{-7}$ and $\beta = 6.3 \times 10^{-6}$ for the asthenosphere and dense body respectively. These β values give the dense body an initial average viscosity of μ and the asthenosphere a viscosity of $10^{-3}\mu$ at $T' = 1$, both equivalent to the temperature-independent models. The dense body viscosity initially varies by two orders of magnitude. The asthenospheric viscosity varies from $10^{-1}\mu$ to 10μ for $0.5 < T' < 0.25$, so asthenosphere which has risen to the Moho would increase to a viscosity in this lower range once it cools.

2.2 Measurements

Models are characterized by measuring the perturbation displacement (w) and velocity ($\dot{w}$) through time. As the initial conditions represent the triggering of a particular mechanism, the velocity at $t = 0$, referred to as the initial velocity $\dot{w}_0$, importantly measures how rapid flow is when the transition from effective stability to instability occurs. A variety of other measurements are taken when the deepest part of the dense body reaches $w' = 1.43$. This reference displacement is typically the end of the initial growth period (Fig. 2) and as the lithosphere has doubled in thickness, is a displacement which is observable in seismological studies (e.g. Zandt *et al.* 2004). The interface between the dense body and asthenosphere is tracked using markers which are advected through time. As instability sinking velocities ($\dot{w}$) typically increase through time (Fig. 2), rates are measured to characterize their acceleration. The exponential growth rate τ, defined in eq. (1), measures how rapidly the sinking velocity initially (generally $w < 1.43$) increases. τ_2 (eq. 2) measures how rapid the super-exponential acceleration is. The typical procedure of fitting τ and τ_2 to the displacement-time curve is used (Houseman & Molnar 1997; Neil & Houseman 1999). The marker which reaches the reference displacement first is used to track these growth rates.

As the initial perturbation is the superposition of multiple wavelengths, this measure of τ' can be an underestimate. We also calculate the growth of the individual invoked waveforms, $w'(\lambda)$, using the discrete cosine transform of the interface markers. When $D' > 0$, we include the wavelengths corresponding to the ten largest terms in the cosine series for a step. Growth-rate measurements of individual waveforms have been benchmarked against the analytic solution of $\tau'(\lambda)$ for $D' = 0$ and $\eta'_c = 1$. We report the largest initial growth rate measured for each instability, which is typically calculated from $w'(\lambda)$ for $D' = 0$ and w' for $D' > 0$. Initial velocity is taken directly from the velocity solution of an instantaneous calculation without time-stepping. This initial calculation begins with only one wavelength, corresponding to the quickest velocity.

Two diagnostic measurements are used to characterize the models as dripping, triggered dripping or delamination. The first is the dense body shear-strain, which should strongly contrast for dripping and delamination. Lagrangian markers are placed on the dense body (Figs 1 and 3), which only record the shear component of the strain tensor. These markers are able to rotate, as well as translate with dense body flow. In the case of ideal bending, when all deformation is accommodated by normal strain in the direction of the bending axis of the dense body, the measured shear-strain should be zero. The measured infinitesimal shear-strain is integrated over each time step.

The second diagnostic measurement for delamination is Moho displacement (Figs 1 and 4). It is measured as the displacement of the initially flat upper surface of the dense body, corresponds to seismic reflectors observed in nature (Levander *et al.* 2011). Its vertical deflection, w_m, is normalized to the perturbation displacement, $w'_m = w_m/w$ and should be close to one for delamination. The purpose of measuring w_m is primarily to quantify whether or not the top of the dense body is peeling away in the models. It should only cautiously be compared to absolute Moho displacement on the Earth, especially if the crust deviates from the extremely strong rheology used in these models and is able to thicken.

Molnar *et al.* (2015) define isostatic and dynamic surface topography as resulting purely from anomalous density and viscous stress respectively. Following this definition, the density field is integrated over a column spanning the entire model height and assuming $w' = 0$, while any deviation from this reference density in other columns results in isostatic variation. These columns are combined to form a profile of isostatic topography. This 'isostatic' topography is a variation of the Airy isostatic model, but applied only to density anomalies arising from changes in thickness of the dense lower crust or mantle lithosphere, rather than buoyant crust. Thickening of the upper crust is negligible, due to its strength, while the lower crust has a neutral buoyancy. Therefore, this measurement predicts subsidence where the lithosphere is thickening. This measurement isolates the isostatic compensation required to accommodate density anomalies at depths below the crust, suitable for comparisons to tomography. It should be treated cautiously for cases where crustal thickness variation dominates the topographic signal instead. The total topographic response, the sum of the dynamic and isostatic components, is calculated by assuming any surface deflection balances the vertical normal stress at the top of the model domain, σ_s.

The instability growth timescales are only predominately dependent on η and η_c if the dense body and decollement dissipate much more energy viscously than the asthenosphere. This is quantified for the dense body by calculating the viscous dissipation, defined as $\eta\dot{\epsilon}^2_{II}$. $\dot{\epsilon}_{II}$ is the second strain-rate invariant and for the calculation of other materials, η is replaced by the relevant material viscosity. This is calculated at many random points within a material, averaged and then compared as a ratio to the total viscous dissipation in the entire model domain at a particular time.

In the temperature-dependent 3-D models, we distinguish between the drip and planar morphology by comparing the largest amplitude from the cosine transform of the vertical velocity

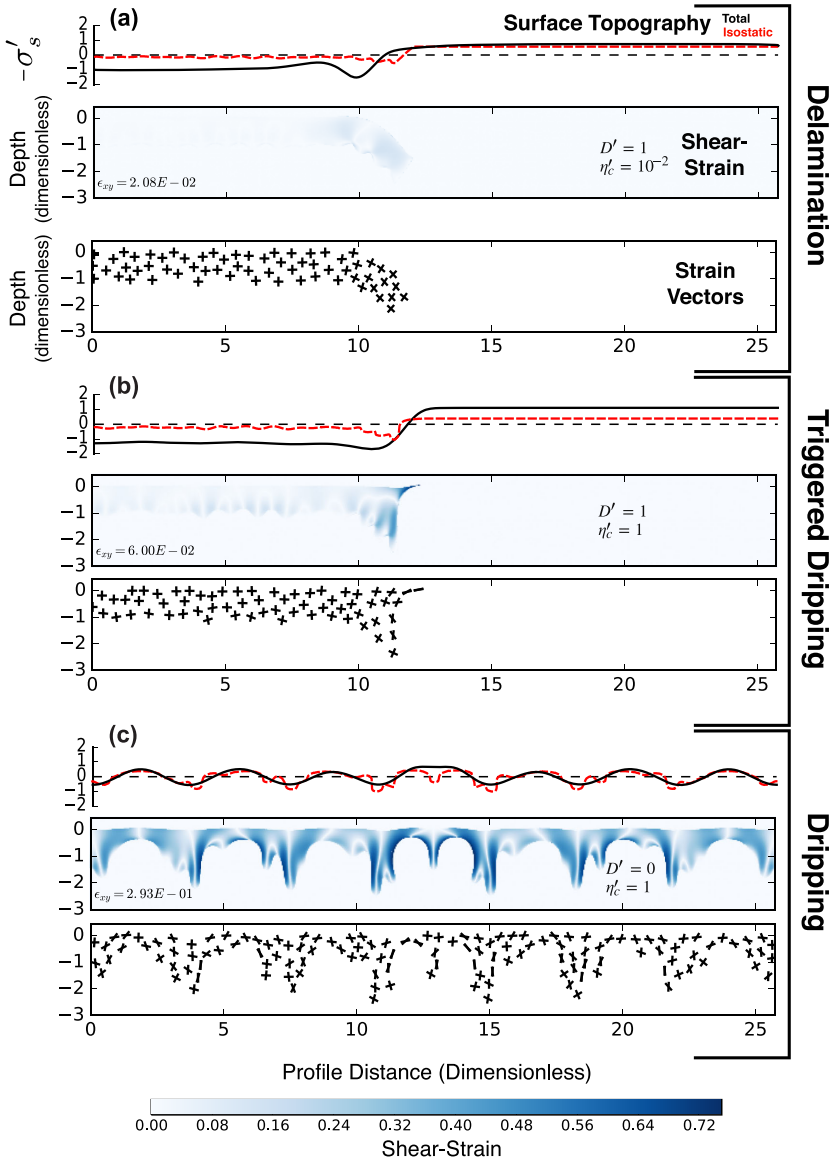

Figure 3. Shear-strain for examples of delamination (a), triggered dripping (b) and dripping (c), with parameters inset. Comparison is made at $w' = 1.43$. Sub-sampled vectors corresponding to the shear-strain measurement are shown, as well as the average shear-strain (ϵ_{xy}) and surface topographic profile for each. Comparison of the isostatic compensation for density anomalies below the crust (red, dashed) and the total topography (black), shows where topography is due to dense body thickness variation. The non-dimensional stress σ'_s can be scaled to a dimensional elevation using a reference stress, $\sigma'_s \Delta\rho L / (\rho_c L')$, where ρ_c is the upper crustal density. Taking $\Delta\rho = 30\,\mathrm{kg\,m^{-3}}$, $\rho_c = 2500\,\mathrm{kg\,m^{-3}}$ and $L = 50\,\mathrm{km}$ gives an elevation of 0.86 σ'_s km. With these dimensions, topography varies by <1 km from the reference elevation.

component in directions parallel and perpendicular to $\hat{s}$ (Fig. 1). The ratio between these should be one for a drip morphology. We also quantify whether or not instability migration occurs in the step direction, by finding the angle between the horizontal velocity component and $\hat{s}$. If migration is dominated by the initial step perturbation, this should be 0°, and larger if 3-D instabilities become prominent. Both of these measures are calculated at the base of the dense body and averaged, also compared at the reference depth.

2.3 Analytic solution and scaling

The analytic method of Neil & Houseman (1999) is used to solve for a RTI which includes the decollement layer. There are two interfaces across which the density contrasts, the asthenosphere-dense body and dense body-decollement interfaces, the latter required to be consistent with the assumption that the decollement material is of reference density. Though there is a density contrast between the upper crust and decollement layers in the numerical models, any perturbation of the interface between the two layers is considered to be negligible, due to the high viscosity of the upper crust. There are therefore two growth-rate solutions, one growing and the other decaying, of which we only take the former. We also solve for the case where the dense body-decollement interface has no initial perturbation, which then has one growing solution.

In order to directly compare the delamination model of Bird (1979) to the RTI, we adjust the delamination model (eq. 3) such that the pressure anomaly at the decollement-asthenosphere interface (ΔP) arises from the anomalous hydrostatic pressure of the dense

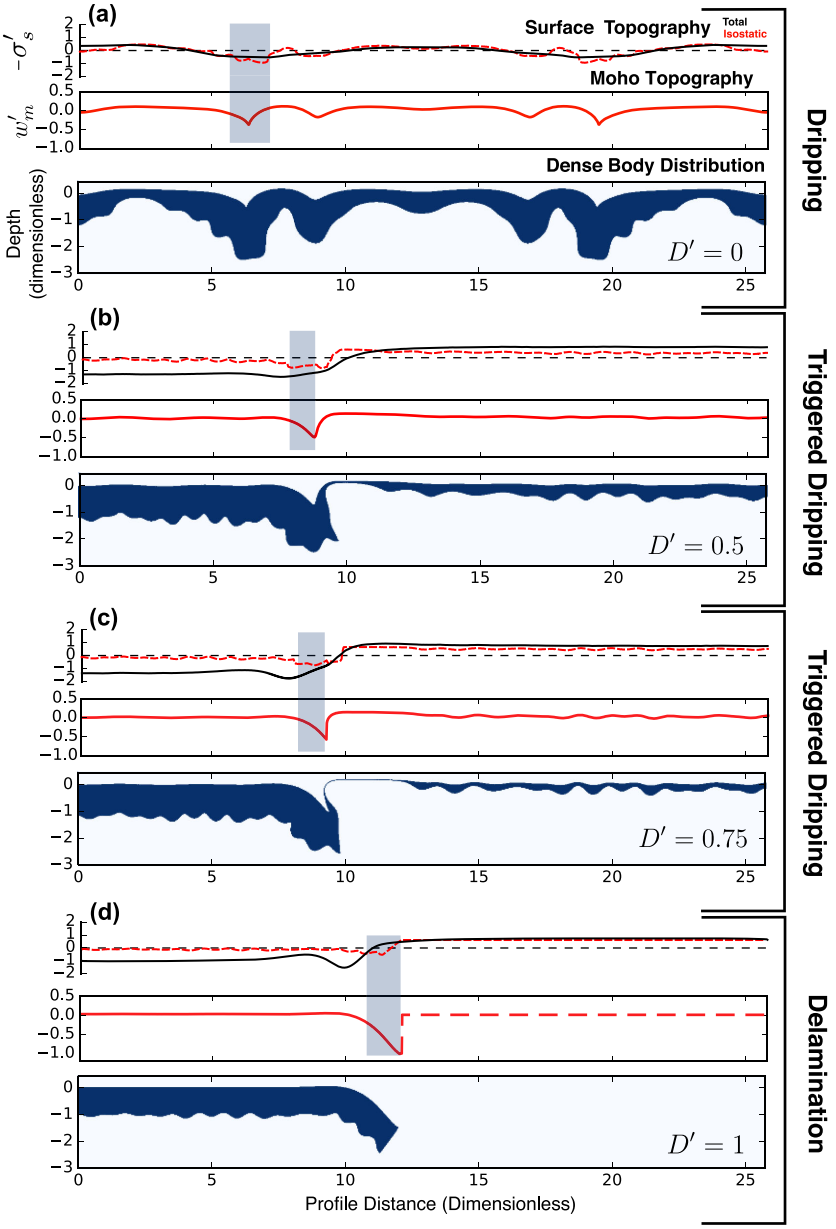

Figure 4. Profiles of surface elevation, depth to the Moho and distribution of dense body directly below, for $\eta_c' = 10^{-2}$ and $D' = 0$ (a, dripping), 0.5 (b, triggered dripping), 0.75 (c, triggered dripping) and 1 (d, delamination). Comparison is made at $w' = 1.43$. The location of subsidence in relation to the dipping Moho and the edge of the dense body subtly contrasts between triggered dripping and delamination, as emphasized by the shaded regions. Comparison of the isostatic compensation for density anomalies below the crust (red, dashed) and the total topography (black), shows where topography is due to dense body thickness variation.

body. This requires the assumption that the anomalous pressure can be represented as a point load on the end of the dense body. We then non-dimensionalize the decollement length scale and viscosity using the dense body as a reference (Table 1). This results in a velocity which is proportional to the buoyancy timescale, $\eta/\Delta\rho g L$, encountered in the RTI (eq. 1). We use this to non-dimensionalize the timescale of the delamination velocity. The non-dimensional velocity then depends only on the ratios of decollement to dense body thickness and viscosity, L_c' and η_c', rather than absolute values (eq. 5). If the delamination velocity varies proportionally to the amount of dense body which has delaminated, as proposed by Bird & Baumgardner (1981), the growth will be exponential and self-similar like the RTI. The exponential growth rate should also then be non-dimensionalized and scaled in the same way as the initial velocity (eq. 5). This formulation is a simple prediction of the delamination growth rate depending on the decollement properties, which we test numerically.

$$\dot{w}_0' \propto \tau' \propto \frac{L_c'^2}{\eta_c'^{\frac{2}{3}}} \tag{5}$$

3 RESULTS

Dripping, triggered dripping and delamination must initially be distinguished in the models, so that their growth rates can later be compared. The two chosen delamination diagnostics, high Moho displacement and low shear-strain, are reproduced only for a small

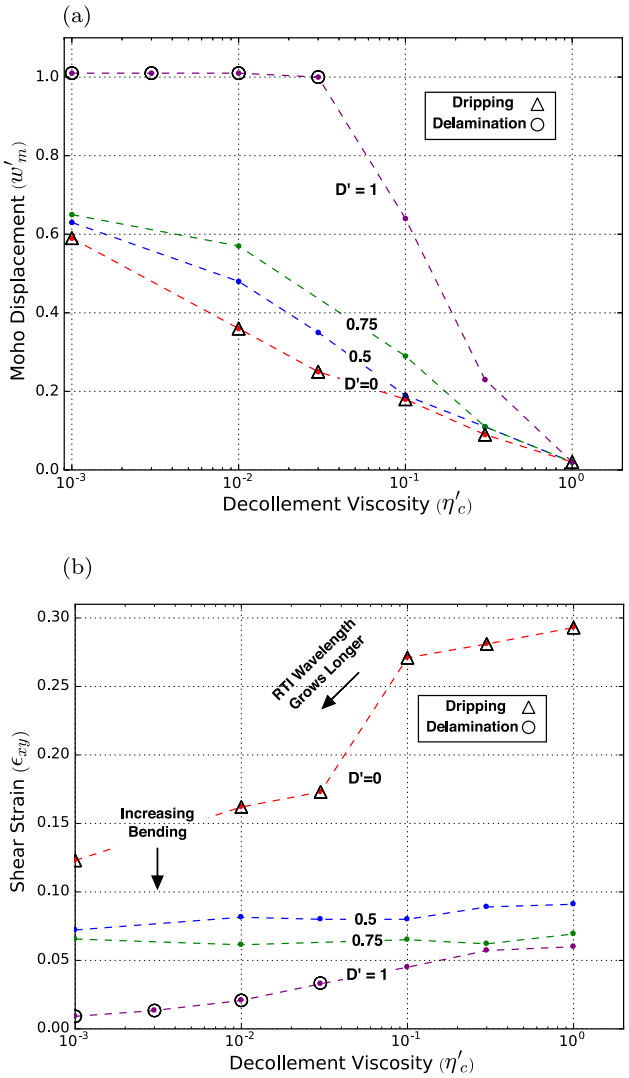

Figure 5. Moho displacement (a) and shear-strain (b) for varied η'_c and D'. Models with $D' = 0$ are characterized as dripping, because of their initial conditions and their excellent agreement with analytic RTI models (Figs 6a and 7). Models are characterized as delamination if $w'_m = 1$ and shear-strain is relatively low. Triggered dripping models, the points not characterized as dripping or delamination, have Moho displacements and shear-strain bearing greater similarity to dripping and delamination respectively.

range of D' and η'_c. The Moho displacement diagnostic of delamination, $w'_m = 1$, only occurs for $D' = 1$ and $\eta'_c \leq 3 \times 10^{-2}$ (Figs 4 and 5). There is a large decrease in Moho displacement for $D' < 1$, marking a change in mechanism from delamination to triggered dripping. The Moho displacement of dripping and triggered dripping can still be <60 per cent of the displacement of delamination, when η'_c is small. With decreasing D', the Moho becomes more cuspate and symmetrical (Fig. 4). Its displacement becomes negligible once $\eta'_c = 1$, even for $D' = 1$, though this would not be the case for denser decollement and crust.

The shear-strain in the models with $w'_m = 1$ is <0.04 (Figs 3 and 5), which is relatively small. Therefore the deformation of models with $D' = 1$ and $\eta'_c \leq 3 \times 10^{-2}$ can be confidently characterized as delamination. Though the delamination shear-strain is small, it is non-zero, most likely because the pure bending assumption (Section 1.2) is only an approximation, as the buoyancy forces do not act on the dense body as a uniform rotation. However, it is still clearly lower than for triggered dripping, which remains relatively constant with decreasing η'_c and for dripping, which is significantly larger.

Dripping shear-strain is relatively large, as expected. It reduces significantly as η'_c decreases, because λ_{max} consequently increases. However, it is still substantially larger than for models with $D' > 0$. Triggered dripping can be distinguished from the end-member models using the Moho displacement and shear-strain (Fig. 5). These measurements do not simply vary between the dripping and delamination end-members in proportion to D'. Instead, the Moho displacement of triggered dripping is similar to that of dripping, yet it deforms with significantly less shear-strain than dripping does. The lower shear-strain is most likely the result of the imposed large wavelength perturbation, because shear-strain becomes negligible for large wavelength flow (Canright & Morris 1993). The instability is also localized to the step, which results in a lower volume of displaced material and therefore potentially a lower average shear-strain. However, there is clearly a greater proportion of low shear-strain markers within the displaced body in the triggered dripping example, compared to dripping (Fig. 3).

3.1 Initial velocity

The dripping, triggered dripping and delamination mechanisms, characterized by their contrasting shear-strain and Moho displacement, also produce contrasting dynamics, from the moment they are triggered (Fig. 6a). The initial velocity ($\dot{w}'_0$) of dripping ($D' = 0$) varies with η'_c, as calculated analytically. The analytic solutions without any initial decollement perturbation provide a better prediction as they match the initial conditions of the numerical models, which for $\dot{w}'_0$ are instantaneous. For triggered dripping ($D' > 0$), the velocity increases by up to an order of magnitude (Fig. 6a). Using the time derivative of eq. (2), this should vary according to $\dot{w}'_0 \propto (w'_0 + D' + 1)^2$. The models with $D' < 1$ agree with this parabolic dependence, which is also predicted by Canright & Morris' (1993) equivalent small amplitude growth equation (eq. 4.1 therein).

When $D' = 1$ and $\eta'_c \leq 10^{-2}$, $\dot{w}'_0$ significantly exceeds the prediction for triggered dripping (Fig. 6a). These models were previously characterized as delamination and the scaling for delamination (eq. 5) accurately predicts the variation of $\dot{w}'_0$ with decreasing η'_c, with a proportionality constant of 0.23. Additional models (not shown) also held $\eta'_c = 10^{-2}$ constant and varied L'_c, to test the proportionality between $\dot{w}'_0$ and L'^2_c. It holds for $L'_c < 0.5$, above which the $\dot{w}'_0 \propto L'^2_c$ scaling overestimates $\dot{w}'_0$. This is likely to be the point at which it can no longer be assumed that the entire thickness of the decollement layer follows the Poiseuille flow model. There is likely to be a lower bound to the scaling, as the decollement becomes too thin for delamination to occur, which was not explored. The proportionality constant is approximately half of the analytically calculated value (eq. 3), though the reason for the discrepancy is unclear.

The initial velocity is indicative of the immediate dynamics following the moment the conditions for a particular mechanism are triggered, for example the event in the eastern Sierra Nevada described earlier, when strain localized 7*Ma* ago (Jones *et al.* 2004; Molnar & Jones 2004). The agreement between the initial delamination velocity and eq. (5) indicates that as soon as the conditions for delamination are generated, the instability instantaneously follows the delamination mechanism. The higher initial velocities with larger D' are also consistent with the models of Canright &

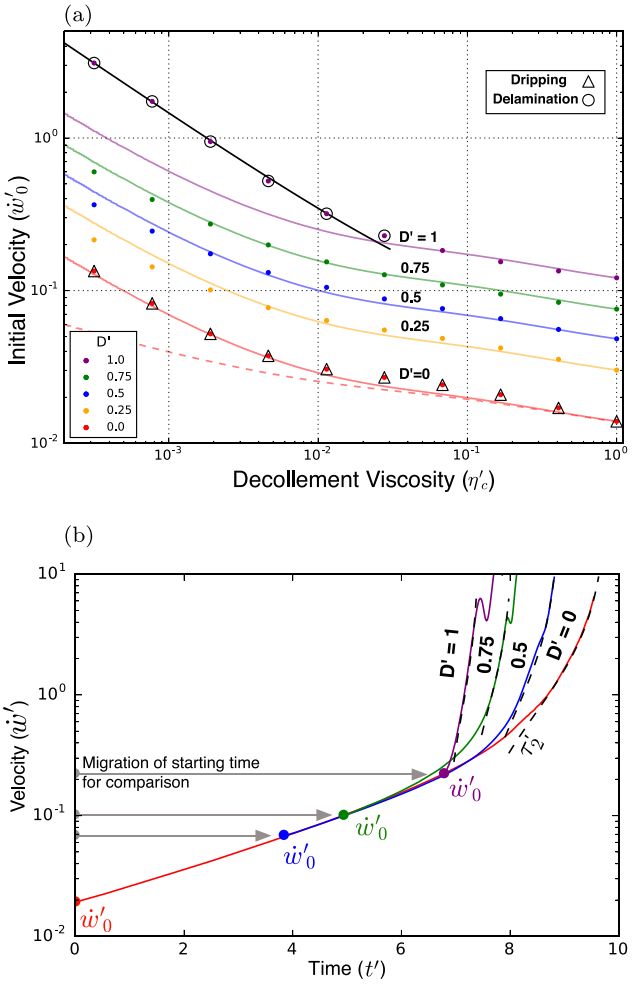

Figure 6. Vertical velocity, measured at the deepest part of the lithosphere-asthenosphere interface at a given time. (a) Initial velocity ($\dot{w}_0$) for varying D' and η'_c, from instantaneous numerical calculations (points) with $w'_0 = 0.085$. The analytic RTI solutions are shown, with (solid red) and without (dashed red) a growing perturbation of the decollement layer. The latter is also scaled empirically from the $D' = 0$ case (solid curves). The analytic delamination scaling (eq. 5, solid black) predicts the correct variation of timescale with η'_c, for the delamination models. (b) Velocity through time for $\eta'_c = 10^{-2}$ and varying D'. Self-similarity of the initial growth period is apparent if the starting times (solid points) of the curves with $D' > 0$ are shifted, to the time at which the dripping model ($D' = 0$) reaches their respective values of $\dot{w}'_0$. Delamination ($D' = 1$) however no longer shares the initial growth rate. At this low η'_c, the super-exponential growth rate τ'_2 clearly increases with increasing D'.

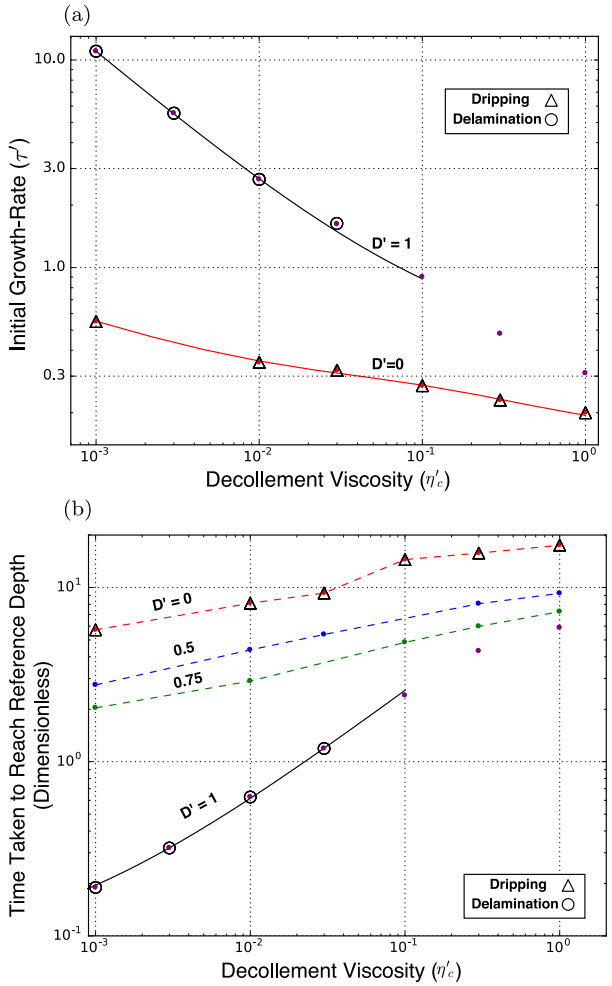

Figure 7. (a) Small displacement exponential growth rate for varying D' and η'_c. The analytic RTI solution with a decollemont perturbation is plotted (red). Triggered dripping ($1 > D' > 0$) models are not shown, as they share the same τ as for dripping. The points for $D' = 1$ and $\eta'_c > 10^{-1}$ are exceptions and show the transition from triggered dripping to delamination models. The delamination models show good agreement with the delamination scaling (black), eq. (5). (b) Time taken to reach the reference depth for models with varying D' and η'_c. The delamination scaling from eq. (5) (solid black) accurately predicts the variation in this time with η'_c. Dashed coloured lines are used purely to mark the model sets for each D'. Time can be dimensionalized, for example by $t/t' = 10\,\mathrm{Ma}$, assuming $\Delta\rho = 30\,\mathrm{kg\,m^{-3}}$, $L = 50$ km and $\eta = 5 \times 10^{21}$ Pa s.

Morris (1993) and Molnar & Jones (2004), where a larger initial perturbation causes the instability to effectively begin closer to the rapid descent phase (Fig. 2), evident from the self-similarity of the curves in Fig. 6(b).

3.2 Growth rate comparison

The analytic small amplitude ($D' = 0$) dripping solution predicts a 3 × increase in the dripping growth rate, as η'_c decreases from 1 to 10^{-3} (Fig. 7). The growth rates of the numerical dripping solutions, measured for the quickest of the growing waveforms measured using Fourier decomposition ($w'(\lambda_{\max})$, Fig. 2), agree with the analytical solution. The analytic solution which allows the decollement to be perturbed, provides the best fit, indicating that thickening of the decollement layer significantly slows down dripping growth rates at low η'_c. As in previous studies (Neil & Houseman 1999), the numerical dripping models grow with the hyperbolic time-dependence described by eq. (2).

Triggered dripping models ($0 < D' < 1$) generally share the initial growth rate of the dripping models ($D' = 0$) at a particular η'_c, which can be clearly observed in the identical initial slopes of plots of $log(\dot{w}')$ over time (Fig. 6b). This self-similarity means that the initial growth of the triggered dripping models begins as if it is starting from a later point in the $D' = 0$ velocity curve and therefore takes less time to reach the rapid super-exponential growth phase (Fig. 2). The self-similarity is still valid at high w' for $\eta'_c = 1$, as all instabilities follow similar timescales of hyperbolic growth, τ'_2 (eq. 2). With decreasing decollement strength η'_c, instabilities with larger D' grow at a quicker super-exponential timescale (Fig. 6b).

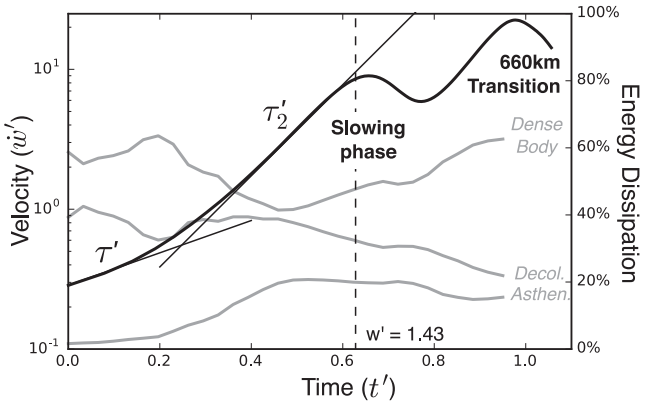

Figure 8. Delamination velocity over time, when $\eta_c' = 10^{-2}$. The two growth phases, τ' and τ_2' are shown (note the logarithmic scale) as well as the time at which the reference depth $w' = 1.43$ is reached. The dimensionless time and velocity could be scaled for the example of $\Delta\rho = 30\,\mathrm{kg\,m^{-3}}$, $L = 50\,\mathrm{km}$ and $\eta = 10^{21}\,\mathrm{Pa\,s}$ as $t = 2.15\,t'\,\mathrm{Ma}$ and $\dot{w} = 2.33\,\dot{w}'\,\mathrm{cm\,yr^{-1}}$. The energy dissipated in each material as a percentage of the total dissipation at a given time (grey) demonstrates the dominating dissipation in the dense body and decollement system, especially during the initial growth.

This hyperbolic timescale varies significantly at $\eta_c' = 10^{-2}$, where $\tau_2' = 0.4$, 0.6, 1.0 and 1.5, for $D' = 0$, 0.5, 0.75 and 1. The transition to super-exponential growth occurs at large w' for the modelled triggered dripping, so variation in τ_2' does not significantly affect the initial instability growth, as described later with Fig. 7(b).

The velocity of a delaminating body increases exponentially (eq. 1), immediately after triggering (Fig. 8), which confirms the hypothesis of Bird & Baumgardner (1981) and agrees with analogue modelling (Bajolet *et al.* 2012). The viscous bending stress therefore appears to vary proportionally with w, during the initial growth phase (τ' in Fig. 8). Delamination quickly progresses into the secondary rapid growth phase (Figs 6b and 8), so comparisons between dripping and delamination growth rates based purely on τ' are an underestimate. It can be used for comparing delamination models however, as τ' and τ_2' vary in the same way with changing η_c'.

Unlike triggered dripping, delamination does not share the same exponential growth rate τ' as the dripping model with an equivalent η_c' (Fig. 7a). Instead τ' is always at least an order of magnitude faster. Additionally, τ' is more sensitive to η_c' than for dripping, resulting in more than two orders of magnitude difference between the two mechanisms for $\eta_c' = 10^{-3}$. The exponential (τ') for delamination varies proportionally to $\eta_c'^{-\frac{2}{3}}$ (Fig. 7a), as predicted by eq. (5). The accuracy of this scaling in describing the variation of $\dot{w}_0'$ and τ supports Bird's (1979) hypothesis that the initial delamination growth occurs by interaction between viscous bending of the dense body and Poiseuille flow in the decollement.

Delamination has an intermittent slowing phase which does not occur in dripping. This slowing phase also appears in triggered dripping for $D' = 0.75$ (Fig. 6b). It is brief though and occurs when the instability has already attained a significant velocity. This slowing phase could result from the increasing curvature of the dense body through time. Previous modelling has shown that subducting sheets peel away from a free-slip upper boundary condition, separated from the slab by a thin low viscosity channel, with a velocity which only increases for a limited period (Ribe 2010, fig. 3b therein). In the case that the slab has a viscosity three orders of magnitude higher than the asthenosphere, as in our models, the slowing occurs at $w' \approx 3$, before returning to a similar rate of increase. This slowing period occurs at approximately twice the displacement as for our models (Fig. 8). However, the qualitative similarity in displacement evolution indicates that the delamination slowing period is related to deformation of the peeling dense body, rather than lower crustal flow.

In order for the velocity of the delaminating dense body to increase, the bending stress must also increase. In the case that the zone of peeling can migrate at an increasing velocity, this can be achieved without progressively increasing the dense body curvature. However, the latter occurs in our models, as well as the equivalent case of Ribe (2010), which may mean that the dense body reaches a point in which further bending is difficult, leading to a maximum sinking velocity. The subsequent velocity increase then may indicate the instability has switched to dripping.

The exponential growth rate τ' is not necessarily the clearest way of comparing the modelled instabilities, as the initial velocities ($\dot{w}'$) also vary, as well as the time taken to reach the rapid super-exponential phase. Instead, the time taken to reach the reference depth $w' = 1.43$, from instability initiation, is a clearer comparison (Fig. 7b). Because triggered dripping and dripping share the same τ' and reach the reference depth before significant super-exponential growth occurs, the growth time varies with η_c' in the same way. Increasing D' for triggered dripping increases $\dot{w}'$ irrespective of η_c' and so the growth time is always reduced, in comparison to dripping, by a constant amount for a specific D'. Delamination has passed through its second growth phase by $w' = 1.43$ (Fig. 8), though because τ_2' varies proportionally to τ', so does the growth time. As a result, the time for delamination to reach the reference depth varies significantly, proportionally to $\eta_c'^{-\frac{2}{3}}$ and can be an order of magnitude shorter than dripping and triggered dripping. The most significant outcome is the difference in growth time between triggered dripping and delamination, even when the initial conditions are similar, evident in the divergence of the curves for $D' = 0.75$ and 1 with decreasing η_c' in Fig. 7(b).

To summarize, dense material can sink at an order of magnitude quicker rate if it is able to delaminate, compared to if it drips. Though delamination begins with a relatively higher velocity than for dripping or triggered dripping, it is the significantly higher exponential growth rate which is primarily responsible for this contrast. For example, as soon as a dense body is perturbed by $D' = 1$, its initial sinking velocity is $\dot{w}'_0 = 0.35$, assuming that a decollement with $\eta_c' = 10^{-2}$ and $L_c' = 0.21$ is present above. For $\Delta\rho = 30\,\mathrm{kg\,m^{-3}}$, $\eta = 10^{22}\,\mathrm{Pa\,s}$, $L = 50\,\mathrm{km}$, this is equivalent to the geologically insignificant rate of $\sim 8 \times 10^{-2}\,\mathrm{cm\,yr^{-1}}$. However, due to the high delamination growth rate, it would only take 14 Ma ($t' = 0.65$, Fig. 7b) for the lithosphere to double in thickness, compared to 183 Ma ($t' = 8.5$) if there is no finite perturbation ($D' = 0$), but the decollement is just as weak.

The time taken to reach the reference depth ($w' = 1.43$) differs significantly between delamination and triggered dripping which is relatively close to the conditions for delamination ($D' = 0.75$). For the example of a decollement with $\eta_c' = 10^{-2}$ and $L_c' = 0.21$, this growth period takes almost five times longer if the finite strain triggering the instability has thinned the dense body by 75 per cent, compared to 100 per cent. The contrast grows to an entire order of magnitude longer, if $\eta_c' = 10^{-3}$. Therefore if geological activity fails to thin the upper 12.5 km of an initially 50 km thick dense body, the instability will take 43 Ma (for $\Delta\rho = 30\,\mathrm{kg\,m^{-3}}$ and $\eta = 10^{22}\,\mathrm{Pa\,s}$) to reach the reference depth and likely be slowed down by thermal

diffusion, instead of growing within the more geologically relevant 4.3 Ma period.

3.3 Timescale comparisons with previous studies

The significant growth rate contrasts between dripping (including triggered) and delamination calculated in Section 3.2 are compared to previous studies. Where studies model the dense lower crust and/or lithosphere with a temperature-dependent density and viscosity, the reported initial geotherm is used to calculate average representative $\Delta\rho$ and η using reported model parameters. In the case of stress-dependent viscosity, η is compared to viscosity plots or calculated based on reported strain-rates. Comparison using these average values is approximate, but provides at least an order of magnitude estimate of the non-dimensional timescale (eq. 1).

The delamination ('DEL') model of Göğüş & Pysklywec (2008) reaches a depth similar to our reference depth delamination approximately 10 × more quickly than for dripping ('DRIP-1'). Accounting for the higher density anomaly in their delamination model, using the timescale non-dimensionalization (Table 1), reduces this to a difference of ∼5×. This is lower than the difference of 16× predicted between delamination at $\eta_c' = 10^{-2}$ and triggered dripping with $\eta_c' = 1$ and $D' = 0.75$. This comparison is justified, as their dripping model appears to begin with a large amplitude perturbation. However, L_c' is twice the thickness of our models, which is predicted using eq. (5) to result in delamination which is 32× faster instead of 5×.

The delamination and dripping models of Göğüş & Pysklywec (2008) also involve the mobilization of different parts of the lithosphere, with contrasting average viscosities which should also affect the relative instability timescales. The lower half of the lithosphere, which is an overestimate of the volume which sinks in the dripping model ('DRIP-1'), has an average viscosity which is $\sim 10^2\times$ weaker than the whole lithosphere, which sinks in the delamination model ('DEL'). This contrast more than compensates for the smaller than predicted timescale contrast between their end-member models. This argument can also partly explain why the dripping ('Drip-2') and delamination ('Delamination-2') models of Wang & Currie (2015) grow at similar timescales. Additionally, L_c' appears to be approximately 75 per cent smaller than the value used by Göğüş & Pysklywec (2008). According to eq. (5), this should slow down delamination relatively by more than an order of magnitude, which could account for the contrast in relative timescales between dripping and delamination, between the two studies.

The rapid delamination timescale calculated ($t' \sim 1$ to reach $w' \approx 1.43$) can be tested against previous studies, using the time non-dimensionalization (Table 1) and delamination scaling (eq. 5). Valera *et al.* (2014) modelled delamination using a Newtonian rheology, as in this study, so a growth-rate timescale can be directly calculated. In their models, it takes 2 − 3 Ma for the delaminating mantle lithosphere to enter the rapid super-exponential acceleration phase, as seen in their measurement of kinetic energy through time (fig. 5 therein). Based on the average dense lithosphere viscosity, thickness and its density relative to the adjacent 'hydrated lithosphere', this time is non-dimensionalized as $0.34 < t' < 0.69$. This is relatively fast compared to the scales typical for dripping and supports our calculation of a rapid delamination growth rate. Our calculated delamination timescale for $\eta_c' = 10^{-2}$, equivalent to their model, is within this range. However, their decollement has $L_c' = 0.28$, which is predicted to alter this range effectively to $0.61 < t' < 1.23$ (eq. 5). Additionally, as it is later shown that viscosity stratification is likely to double the growth time, their delamination model would be approximately 2× slower than in this study. However, their delaminating body is adjacent to a zone of thinner lithosphere and strong lower crust, which is likely to generate slower delamination than the ideal case modelled here.

The models of Stern *et al.* (2013) also use a Newtonian rheology and have already been non-dimensionalized. Because their lower crustal viscosity is $\eta_c' = 10^{-1}$, their models are not predicted to reach the rapid descent as quickly as delamination, instead $t' > 1$ (Fig. 7b). Accounting for our definition of L being the dense body thickness, $w' = 1.43$ is approximately reached by $t' \approx 12$. At $\eta_c' = 10^{-1}$, we have calculated $t' = 2.5$ and 5, for $D' = 0.75$ and 1 respectively, giving bounds for their initial condition of $D' = 0.85$. Their slower calculated growth time can be partly explained by taking into account their assumption of $L_c' = 0.14$, compared to $L_c' = 0.21$ used in this study. Using eq. (5), this slows our predicted range to $6 < t' < 12$. Additionally, it is later shown that temperature-dependent viscosity stratification of the dense body approximately doubles the instability timescale for delamination. The slowing effect for triggered dripping would be slightly less, as only the lower part of the lithosphere initially deforms. Taking this into account, the timescale calculated in Stern *et al.* (2013) for $D' = 0.85$, is slightly faster than our calculation for triggered dripping at $D' = 0.75$, showing good agreement.

As the models of Bajolet *et al.* (2012) generally assume that $\eta_c' = 10^{-3}$, their observations can be used to test the extremely rapid corresponding timescale predicted here (Fig. 7). Unlike our study and all other studies used for comparison, analogue models were used for their analysis. Therefore, comparisons to their results also test for agreement between numerical and analogue approaches for modelling instabilities. After non-dimensionalization using their described parameters, their reference experiment 'DEL10' reaches approximately our reference depth of $w' = 1.43$ after $t' = 7.2 \times 10^{-2}$. Accounting for their slightly thicker decollement $L_c' = 0.26$ using eq. (5), slows this down to $t' = 0.11$ at $L_c' = 0.21$, which is the same extremely rapid order of magnitude calculated here for $\eta_c' = 10^{-3}$.

Bajolet *et al.* (2012) also varied $\Delta\rho$ (comparing 'DEL10' and 'DEL19'), demonstrating (fig. 10 therein) that the instability timescale is approximately proportional to it, which agrees with our non-dimensionalization. They additionally showed that doubling the thickness of the decollement ('DEL14' compared to 'DEL10') decreases the time taken to reach $w' \approx 1.43$ by 40 per cent. This is less than our prediction of 75 per cent, however it is difficult to be confident of the exact discrepancy given the slight differences in the initial perturbation size between these two models.

The majority of existing models of delamination often use complex rheologies, which make it difficult to estimate an effective viscosity for non-dimensionalization. However, the effective viscosity required for a non-dimensionalized model timescale to agree with our modelled timescales (Fig. 7) can be approximately calculated and checked for plausibility. In order for the delamination model ('DEL') of Göğüş & Pysklywec (2008) to grow at the predicted timescale for $\eta_c' = 10^{-2}$, the dense body viscosity would need to have been approximately $\mu \sim 5 \times 10^{21}$ Pa s. Considering that the L_c' used is approximately twice the thickness used in this study, this becomes $\mu \sim 10^{22}$ Pa s. Their rheological law reproduces this effective viscosity for strain-rates in the order of $\sim 10^{-14}$ s^{-1}, which is at the higher end of their reported range. Therefore, the nonlinear rheology is important for reducing the effective viscosity and allowing delamination to occur within 5 Ma.

A similar comparison can be made to the delamination model of Krystopowicz & Currie (2013), which takes approximately 2.5 Ma for delamination to occur (comparing 32.5 and 35 Ma in 'Model 2' therein). This requires an effective viscosity in the order of 10^{21} Pa s when comparing to our equivalent non-dimensionalized timescale for $\eta_c' = 10^{-2}$. This is an order of magnitude weaker than their calculated rheology for the assumed initial shortening rate (Fig. 1b therein), though the mantle lithosphere has clearly weakened to this order of magnitude at its mid-thickness, during instability. The contrast in effective viscosity between the models of Göğüş & Pysklywec (2008) and Krystopowicz & Currie (2013) results from the assumed higher $\Delta\rho$, L_c and L in the former.

3.4 Energy dissipation

In scaling delamination by the viscosity of the dense body, rather than that of the asthenosphere, we have followed the assumptions of Bird (1979) that the delamination velocity is primarily limited by flow of the decollement and dense body. The converse is that the asthenosphere provides the only non-negligible resistance, so that delamination would then be modelled by 'Stokes creeping flow' (Capitanio *et al.* 2007). The dependence of delamination timescales on η_c' favours the former model, but we need to test whether the latter is also occurring. A simple way to quantify which system, the lithosphere or asthenosphere, the delamination velocity is most sensitive to, is to compare the energy dissipated by viscous flow for each material.

During the first exponential growth phase, the dense body and decollement account for more than 95 per cent of the total energy dissipation (Fig. 8). Dissipation by the asthenosphere increases to ~20 per cent during the quicker second phase, but this is still only a minor role. The dissipation in the first half of the instability's growth is consistent with the model that the increasing velocity occurs due to quicker bending of the dense body and Poiseuille flow in the decollement. In the second half, dissipation in the dense body dominates over that of the decollement, until it is 60 per cent of the total dissipation as it nears the 660 km transition. This also corresponds to the brief slowing phase, which may mean that the growth switches to a mode in which the sunken dense body is deforming, potentially transitioning to dripping, more than it is decoupling. This could be because the bending velocity is unable to maintain its acceleration, or because deformation of the delaminated portion becomes more efficient than further peeling. Delamination is therefore controlled by lithospheric dynamics, rather than the asthenosphere, even at high displacement. Scaling by η and η_c' holds and the initial delamination growth, before it reaches the lower mantle transition, should not be modelled as 'Stokes creeping flow'.

3.5 Surface and moho topography

Our results are consistent with previous analyses distinguishing dripping and delamination based on surface topography (Göğüş & Pysklywec 2008; Wang & Currie 2015). Dripping and delamination produce surface topography of contrasting morphology and magnitude (Figs 3 and 4). Delamination generates subsidence and uplift which are about 3 × and 1.5 × greater respectively than dripping, which is similar to the observations of Göğüş & Pysklywec (2008) and Wang & Currie (2015). As also observed in previous studies, delamination generates an asymmetric step from subsidence to uplift, above the sinking end of the dense body, which contrasts the symmetrical topography of dripping. The asymmetric step in topography for delamination is superimposed onto large wavelength zones of subsidence and uplift, corresponding to the initial asymmetry in the dense body thickness. In reality, the large wavelength zone of uplift by delamination would be limited to a finite region, depending on how wide the initial zone of lithospheric thinning or weakness is, as in Göğüş & Pysklywec (2008).

Triggered dripping would be characterized as delamination, if the previous surface topography diagnostics of delamination (Göğüş & Pysklywec 2008; Wang & Currie 2015) are used. Like delamination, triggered dripping generates an asymmetric step from subsidence to uplift, above the sinking dense body and rising asthenosphere respectively. This similarity between triggered dripping and delamination results from the similar asymmetric step imposed in the initial conditions. Significant horizontal migration of this asymmetric topographic step in topography also occurs for triggered dripping, generally over a distance of $3L$ by $w' = 1.43$. This migration, qualitatively characteristic of delamination, is actually 50 per cent higher than for delamination. This difference is likely to occur due to delamination's increase of dense body curvature, which has been hypothesized to limit further peeling (Section 3.2).

The similarity in the magnitude of uplift and subsidence, between triggered dripping and delamination, is surprising given their contrast in growth rate, τ. It takes ~7× longer for the lithosphere to double in thickness by triggered dripping with $D' = 0.5$, compared to delamination. The component of topography resulting from viscous stresses would therefore be expected to be significantly higher for delamination. The similarity in their topographic magnitude may be the result of a difference in growth mechanisms: because the dense body thickens significantly for triggered dripping, isostatic compensation results in a similar magnitude of subsidence as the quicker delamination, which instead has negligible dense body thickening (Figs 3 and 4). The similarity in topographic magnitude may also be due to a difference in the way viscous stress is distributed through the dense body.

There are subtle differences in surface topographic morphology between triggered dripping and delamination. Subsidence due to triggered dripping occurs above the region with the highest dense body displacement (w) and thickening. This is expected, given that the thickened dense body requires isostatic compensation. Subsidence does not occur above the region of highest w, instead above the region where the dense body is actively peeling away from the decollement (Fig. 4, at the profile distance $10L$), where the highest dense body bending stresses are. The strain-rate in the dense body (not shown) is the highest directly below the zone of localized subsidence and rapidly decays away from this zone.

This contrast could possibly distinguish triggered dripping and delamination in nature, by locating the region of highest w and w_m and checking whether the surface above is subsiding or uplifting (shaded, Fig. 4). This zone will be subsiding for triggered dripping and the crust may potentially thicken, whereas it will be uplifting for delamination, with asthenosphere flowing in towards the lower crust. This diagnostic for triggered dripping becomes complicated if the crust is weak enough to thicken above the thickening dense body, as this can generate uplift instead (Neil & Houseman 1999). In this case, the inference of symmetrically dipping Moho reflectors, the 'V-shaped' Moho, could be used to identify triggered dripping, as suggested by Zandt *et al.* (2004). Though the V-shaped Moho occurs for $D' = 0.5$, it becomes asymmetrical for $D' = 0.75$ and the dipping Moho closest to the dense body edge would not be detectable due to its high angle (Fig. 4).

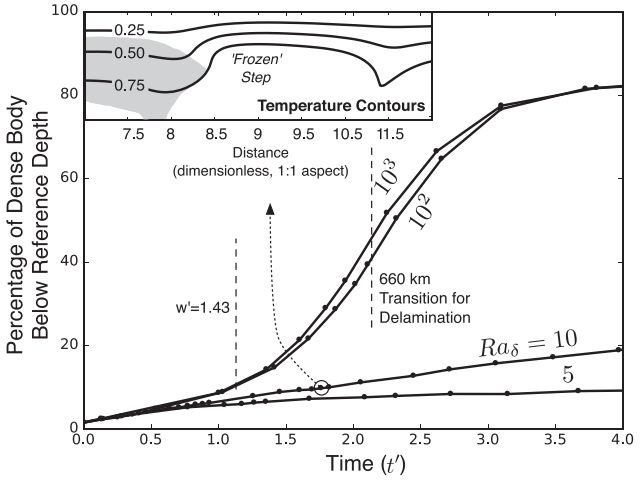

Figure 9. Percentage of material which has sunk past the depth corresponding to the initial base of the dense body, for varying boundary layer Rayleigh numbers. Models were 2-D and used $\eta_c' = 10^{-2}$, $D' = 1$ and temperature-dependent density and viscosity. Delamination switches to dripping for $Ra_\delta \leq 10$ (eq. 4), as shown inset for a particular time-step from $Ra_\delta = 10$. In this example, the wedge zone above the displaced dense body (the latter shaded) has cooled and further peeling is prevented. Temperature contours are labelled as fractions of the potential mantle temperature.

3.6 2-D temperature-dependent models

The effects of thermal diffusion are explored using a secondary set of temperature-dependent models, described in Section 2.1. Thermal diffusion can potentially halt delamination and force it to switch to dripping or it can cause a morphology switch from planar to drip. In the 2-D temperature-dependent models, the former occurs if asthenosphere flowing into the lower crust above the peeling dense body cools quickly enough to raise the viscosity of the decollement zone. If this happens, the dense body has peeled away by a small amount and stalled, the in-flowing asthenosphere above it has a cooling geotherm and the base of the dense body transitions to dripping (Fig. 9). As this dripping only recycles part of the dense body, the persistence of delamination is measured by the volume of material sinking through time. From this measurement, only the models with $Ra_\delta \geq 10^2$ (eq. 4) developed by persisting delamination. The cooling asthenosphere is able to cool to the range of $10^{-1}\eta$ to η at the Moho, so the decollement region will no longer satisfy the $10^{-2}\eta$ viscosity requirement for delamination. The stalling of delamination in this way then depends on whether or not delamination is sufficiently quicker than thermal diffusion, which is quantified by the Ra_δ threshold. When the delaminating body has reached the base of the model, which takes about twice as long as for the temperature-independent models (comparing Figs 8 and 9), the high rate of recycling slows down for $\Delta t' \sim 1$. By this time, delamination has recycled at least four times more material than the models which have transitioned to dripping.

If delamination can only persist when $Ra_\delta \geq 10^2$ (eq. 4), there should be a minimum required growth rate for a delaminating instability. This time is dimensionalized as $t = t'L^2/(Ra_\delta \kappa)$. As it takes $t' = 2.1$ for a delaminating body to reach the base of the model domain in the temperature-dependent models (Fig. 9) and assuming that $L = 50$ km and $\kappa = 10^{-6}$ m^2 s^{-1}, a delaminating body is required to be recycled within 1.7 Ma or less. For $\Delta\rho = 30$ kg m^{-3}, the dense body viscosity must be 3.7×10^{20} Pa s or weaker. This timescale and viscosity could both be slightly larger, as the minimum Ra_δ is only known to an order of magnitude. As discussed in Section 3.2, once the conditions for delamination initiation are met in previous models, it has been modelled as taking only ~2 Ma for the dense body to peel away and break off (Göğüş & Pysklywec 2008; Krystopowicz & Currie 2013).

κ and L can vary between previous studies, so the more precise measurement for comparison is Ra_δ (eq. 4). $Ra_\delta \approx 680$, 320 and 80 for 'DEL' by Göğüş & Pysklywec (2008), 'Delamination-2' by Wang & Currie (2015) and 'Model 2' by Krystopowicz & Currie (2013) respectively. The estimates for 'DEL' and 'Model 2' are calculated using average dense body parameters, as in Section 3.3. A representative effective viscosity is not reported for 'Delamination-2', so Ra_δ is calculated as $Ra_\delta = t_{1.43}L^2/\kappa$, where $t_{1.43}$ is an approximate estimate for the time taken for their model to reach $w' \approx 1.43$. In this case it is assumed that the equivalent non-dimensional time is ~1 for delamination.

The delamination models of Göğüş & Pysklywec (2008), Wang & Currie (2015) and Krystopowicz & Currie (2013) each show negligible cooling of the lower crust immediately after the mantle lithosphere has peeled away, which is the behaviour predicted for Ra_δ above the critical threshold, which is somewhere $10 < Ra_\delta < 10^2$. The first two studies certainly meet this criteria, while the third is closer to the threshold, but could plausibly satisfy it. $Ra_\delta \approx 25$ for the delamination models of Valera *et al.* (2014), calculated from eq. 4 using their reported model parameters (as in Section 3.3). This is much closer to the critical Ra_δ threshold and plausibly below it, indicating that thermal diffusion may be prominent. In their delamination models, the region directly above the peeling lithosphere is significantly colder than the asthenosphere, in a similar way to Fig. 9 (inset), indicating that thermal diffusion is occurring more quickly than delamination.

The delamination in Valera *et al.* (2014) initially involves rapid peeling of the upper mantle lithosphere during the initial 6 Ma, before the lithosphere stops peeling and the instability flow is dominated by dripping of the lower lithosphere (fig. 3 therein). After 12 Ma, the displaced Moho is frozen and the lithosphere below has thickened, in a similar way to our equivalent instability with $Ra_\delta = 10$ (eq. 4 and Fig. 9, inset). Therefore, our critical boundary layer Rayleigh number can successfully describe why delamination persists in some models (e.g. Göğüş & Pysklywec 2008) and not others (Valera *et al.* 2014).

3.7 3-D temperature-dependent models

The transition from planar to drip morphology (Fig. 1, inset) is quantified using 3-D models of triggered dripping with varying D', where D' is now the dimensionless amplitude of an initial planar perturbation. Small amplitude ($w' < 0.1$) 3-D drip perturbations are included and typically dominate over the initial planar perturbation only if D' is relatively small, as in Fig. 11(a) ($D' = 0$). The focus is on the persistence of the planar morphology of a triggered dripping instability. Delamination was not studied in 3-D, though if a planar morphology can persist for the initial growth of triggered dripping, this will also be the case for delamination. The initial step perturbation of size D' has a planar morphology, so the transition to a drip morphology during the initial growth becomes less likely with increasing D' (Figs 10 and 11a). This persistence of the planar morphology, compared for varying D' and $\eta_c' = 10^{-2}$, is observed as both migration in the step direction ($\hat{s}$) and vertical flow with a dominantly planar morphology. The D' threshold for persisting planar morphology is approximately $D' = 0.3$. Therefore if a dense body is decoupled from the upper crust (low η_c'), it requires a planar

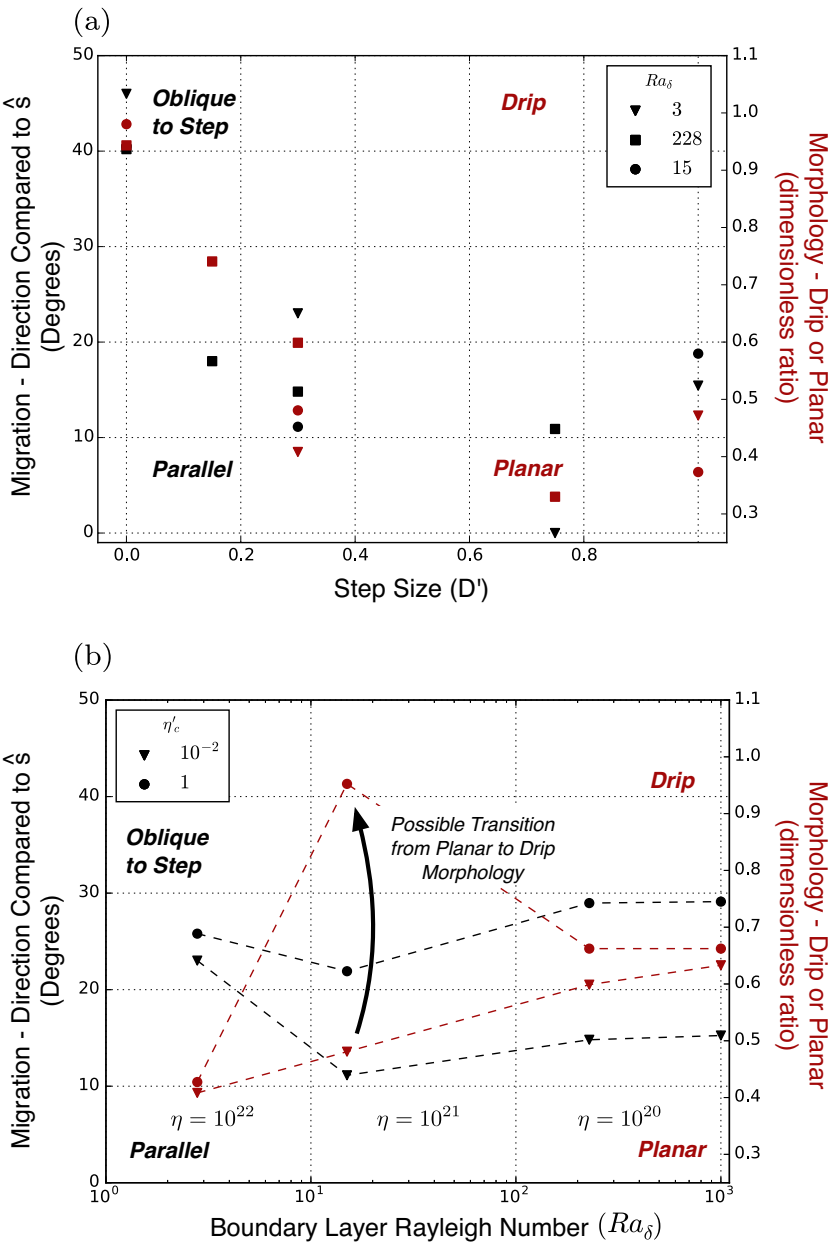

Figure 10. Measures of how '3-D' the instability morphology and migration are, for varying D', η'_c and Ra_δ (eq. 4). The models with varying Ra_δ and η'_c (b) have a constant $D' = 0.3$, which is the lowest D' preventing significant morphology transition (a). A significant switch to the drip morphology occurs near $Ra_\delta = 10$ (b), if $\eta'_c = 1$. This switch is clearly dependent on η'_c, so a change in rheology, marked with an arrow, may potentially produce the transition from a planar to drip morphology. The corresponding η for a range of Ra_δ are shown in Pa s, assuming $\Delta\rho = 30\,\mathrm{kg\,m^{-3}}$, $L = 50\,\mathrm{km}$ and $\kappa = 10^{-6}\,\mathrm{m^2\,s^{-1}}$.

perturbation which is at least a third of its thickness, in order to grow with a planar morphology. The dependence of these measurements on Ra_δ (eq. 4) is secondary to D' for this decoupled case.

When the dense body is decoupled ($\eta'_c = 10^{-2}$), a decrease in Ra_δ (eq. 4) and therefore an increase in the influence of thermal diffusion, actually results in increased persistence of planar structures (Fig. 10). This is due to the thermal erasure of small wavelength perturbations compared to the invoked large wavelength 3-D perturbation. Thermal diffusion however also acts to slow the growth of the 2-D step, when $Ra_\delta \leq 3$, resulting in the superposition of drips over the large wavelength planar step. This Ra_δ results in significant formation of a dense thermal boundary layer beneath the dense body, though the sinking velocity at the dense body edge has generally overtaken the rate of diffusion by the time of measurement at $w' = 1$.

Coupling of the dense body to the crust, $\eta'_c = 1$, reduces the persistence of planar structures (Fig. 10). This effect is significant for $Ra_\delta = 15$ (eq. 4 and Fig. 11b), which appears to be a specific point at which the coupled instability is slowed enough for dripping to dominate, but not enough for the dripping wavelengths to be erased. The transition from planar to drip morphology in this case occurs immediately, so that migration is negligible.

4 DISCUSSION

The sinking velocity of dense lower crust and/or mantle lithosphere which is delaminating, grows exponentially at a rate which

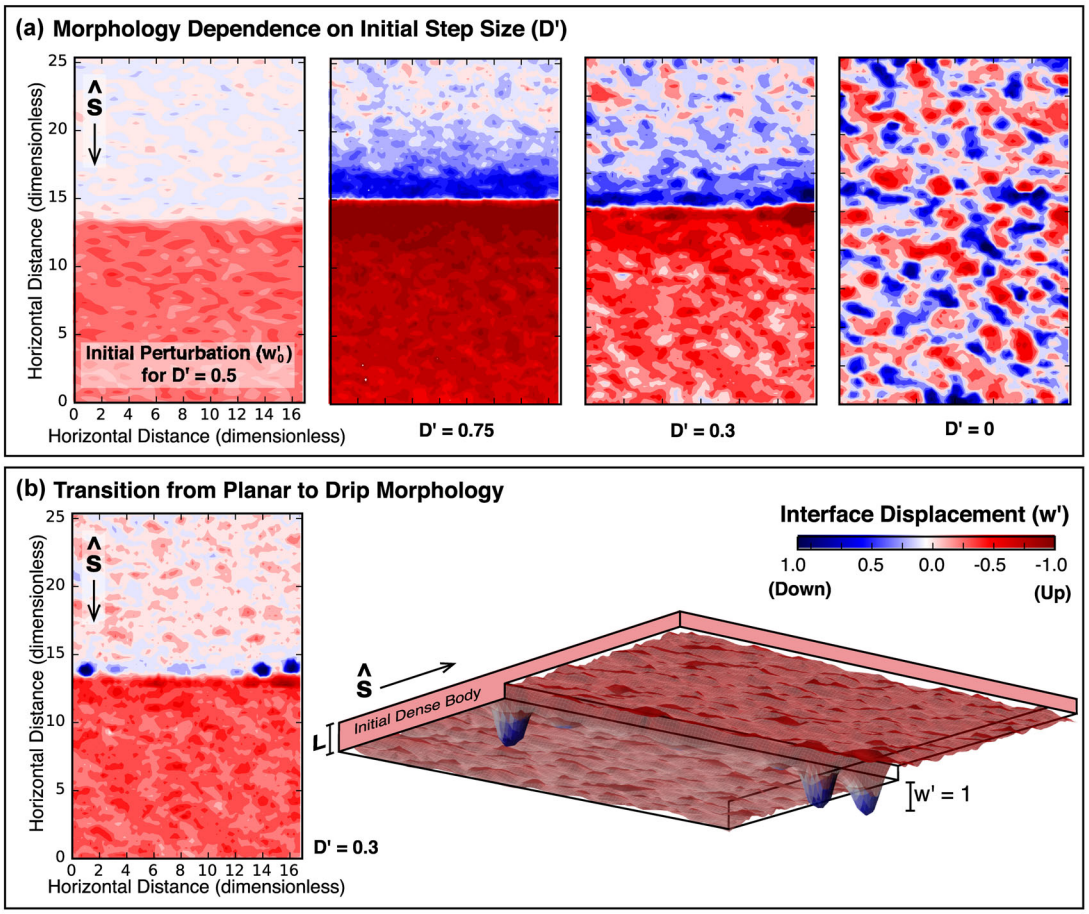

Figure 11. Perturbation displacement (w') of representative 3-D models, for varying η_c', D' and Ra_δ (eq. 4). Comparisons are made when $w' = 1$ is first reached. For these temperature-dependent 3-D models, w' is measured as displacement of the ΔT isotherm from the reference depth L, which is the initial base of the unperturbed dense body. (a) Morphology dependence on D', all with $\eta_c' = 10^{-2}$ and $Ra_\delta = 228$. An example of the initial geometry is shown (left) for $D' = 0.5$. For these η_c' and Ra_δ, an initial step size of $D' = 0.3$ is sufficient for the instability to sustain a planar morphology until $w' = 1$ (as in Fig. 10a). (b) For the case $Ra_\delta = 15$ and $\eta_c' = 10^{-2}$, the dense body switches from an initially planar morphology (right, shaded pink polygon), to a drip morphology during the time it takes to reach $w' = 1$. In comparison to the $D' = 0.3$ case above (a), the combination of a stronger decollement and lower Ra_δ is responsible for the contrast in morphology at $w' = 1$ (as in Fig. 10b). The interface displacement is also plotted as an equivalent 3-D surface (right). The 3-D surface colours have been shaded to emphasize the drip morphology and so differ slightly to the 2-D representations and corresponding colour bar. The $\hat{s}$ vector shows the model orientation, as defined in Fig. 1.

is typically an order of magnitude quicker than for dripping or triggered dripping. This means that material which would typically take 100 Ma to reach a significant velocity by dripping, could delaminate on the 10 Ma scale. Therefore strong materials, such as pyroxene-dominated restites (Bystricky & Mackwell 2001) or the cold upper part of the mantle lithosphere following an Arrhenius rheology, can be recycled without requiring extreme degrees of weakening, if the appropriate initial conditions are triggered.

Molnar & Jones (2004) showed that the plausibly high strength of the dense lower crust beneath the Sierra Nevada (western USA) is difficult to reconcile with its rapid recycling timescale, unless the body was thinned by at least 50 per cent prior to instability. Though the equivalent initial condition of $D' = 0.5$ in our models (triggered dripping) also results in a shorter time frame for recycling, this acceleration is much more significant if delamination occurs. The modelled instabilities grow by triggered dripping, rather than delamination, when there is even a thin layer of mantle lithosphere separating the asthenosphere from the thickening decollement layer above the end of the sinking dense body (Fig. 4b). The ability to recycle strong material is therefore highly sensitive to whether or not the dense lower crust and/or mantle lithosphere has been completely thinned ($D' = 1$) prior to instability initiation.

The timescale at which a delaminating body first reaches a significant displacement is highly variable, but appears to depend simply on groups of key parameters. These can be used to predict a variety of delamination behaviour and potentially explain differences between previous studies. As with dripping, the delamination timescale is likely to scale with the characteristic buoyancy flow-rate scale $\Delta\rho g L/\eta$. η has the greatest natural variability, particularly as a result of its exponential temperature dependence. Though it is the quickest instability mechanism modelled here, the timescale of delamination can still therefore be limited by the effective viscosity of the delaminating material. Comparison of previous studies (Section 3.3) indicates that the effective viscosity controlling the instability timescales of the rapid delamination models of Göğüş & Pysklywec (2008) and Krystopowicz & Currie (2013) corresponds to their reported rheology parameters when weakening by stress-dependence or plasticity is significant. Without such weakening, the viscosity contrast between the upper and lower mantle lithosphere could possibly offset the higher growth

rate of delamination, compared to dripping. In this case, dripping of the weaker lower lithosphere may be the dominant instability, as is typical for an Arrhenius rheology if only dripping is considered (Conrad & Molnar 1999). However, these two mechanisms are not mutually exclusive, as modelled delamination is often triggered by such dripping (Krystopowicz & Currie 2013; Wang & Currie 2015), which occurs initially and weakens or perturbs the lithosphere. Additionally, Krystopowicz & Currie (2013) showed that weakening can lead to the delaminating mantle lithosphere breaking off, resulting in an episodic cycle of dripping, weakening, delamination and then break-off.

If the dense body's viscosity has a negligible influence on the delamination growth rate, as previously proposed (Le Pourhiet *et al.* 2006), then the instability timescale once delamination has been initiated would reflect the asthenospheric rheology, rather than that of the crust and mantle lithosphere. Because our models viscously dissipate a much higher percentage of the gravitational energy than the asthenosphere, any inferred instability timescale could be used to infer the dominating lithospheric viscosity, as has been done for dripping and triggered dripping (Molnar & Jones 2004; Stern *et al.* 2013). Ribe (2010) showed that the velocity of a freely subducting slab only depends on the slab viscosity when it is significantly higher than that of the asthenosphere. The argument that asthenospheric viscous dissipation dominates (Le Pourhiet *et al.* 2006) may then only hold when the lithosphere has weakened to within two orders of magnitude of the asthenospheric viscosity, which is sufficiently weak in Capitanio *et al.* (2007).

In addition to the existence of a lower crustal strength criteria for delamination to be initiated, the strength and thickness of the lower crust results in delamination at a range of timescales, appearing to scale with $L_c'^{\,2}/\eta_c'^{\,\frac{2}{3}}$. This has been used, for example, to argue that the relatively rapid non-dimensional timescales of Bajolet *et al.* (2012) are the result of a small η_c' (Section 3.3). A significant contrast in the choice of L_c' may also explain why delamination is faster than dripping in the models of Göğüş & Pysklywec (2008), but not in Wang & Currie (2015). These parameters are often not explicitly set (Morency & Doin 2004; Le Pourhiet *et al.* 2006), instead effectively depending on dynamic conditions, such as strain-localization. In these cases, there is an effective lower-crustal cohesion or stress exponent which is responsible for the modelled delamination timescale.

Depending on whether the boundary layer Rayleigh number Ra_δ (eq. 4) exceeds a critical value, delamination may begin, but quickly stall and switch to dripping. This is not a common occurrence in delamination models, primarily because the choice of model parameters typically result in $Ra_\delta \sim 100$ or above (Göğüş & Pysklywec 2008; Krystopowicz & Currie 2013; Wang & Currie 2015), which is clearly sufficient for delamination to persist. The models of Valera *et al.* (2014), however are set up with a Ra_δ which is close to $Ra_\delta = 10$, which results in stalling of our modelled delamination. The subsequent prediction, that thermal diffusion is prominent and leads to stalling, is supported by their model evolution, which begins with delamination, before the mantle lithosphere stops peeling and its lower part drips instead. This transition, shared by our equivalent stalling model (Fig. 9, inset), results in a displaced, asymmetric Moho which is diagnostic of delamination, but also a high degree of internal shear-strain, diagnostic of dripping. This bears similarity to the seismological study of the dense body hanging beneath the Colorado Plateau (Levander *et al.* 2011), which may therefore have undergone such stalling. Though the relative viscous and thermal timescales are appropriate for stalling in the models of Valera *et al.* (2014), the decollement has a finite extent in their models, which may also be responsible for the stalling. This alternative hypothesis could be tested further using models with a varying decollement extent. Additionally, the slowing effect associated with stalling could possibly be compensated in nature, if lithospheric weakening occurs at high displacement (Krystopowicz & Currie 2013). Regardless, stalling is another manifestation of the significant contrast between the dripping and delamination growth rates. Without this contrast, an instability switching from delamination to dripping would continue to be recycled at a relatively high velocity, due to its high displacement.

4.1 Triggered dripping versus delamination

We have identified a mechanism which is a mixture of the dripping and delamination end-members, called triggered dripping. It is similar to dripping in its growth rate, but resembles delamination in appearance. This has implications for linking observations to instability dynamics. Each of the diagnostics which distinguish delamination from dripping, are also common to triggered dripping. The similarity is due to the similar initial conditions and subsequent deformation. There is a fundamental difference however in what causes each instability to accelerate: as with dripping, triggered dripping thickens the dense body in order to increase the normal stress responsible for instability growth. Delamination involves negligible thickening, instead accelerating because the increasing load of dense body which has peeled away from the upper crust is balanced by quicker bending of the dense body which is actively peeling. Dense body which has peeled away from the crust but shows evidence that it is thickening, has switched to triggered dripping, based upon our definition of delamination. The implication from our mechanism characterization is that this switch would result in a significant decrease in the instability growth rate. Aside from this change in timescale, the surface topography and dense body geometry would still resemble delamination, making mechanism diagnosis difficult.

Viscosity calculated assuming that dripping or triggered dripping is the responsible mechanism, for example in Molnar & Jones (2004), could be overestimated by an order of magnitude if the dominating instability mechanism is actually delamination. Given the difficulty in distinguishing triggered dripping from delamination, this introduces a significant uncertainty into rheological inference. The initial conditions required for triggered dripping or delamination can also be indistinguishable, so this uncertainty in instability dynamics may simply be unavoidable.

There are subtle contrasts between triggered dripping and delamination which are worth pursuing, but are difficult to apply in practice. Any observation of uplift directly above a sinking body can be explained by delamination or by dripping which involves thickening of buoyant crust (Neil & Houseman 1999). If the dense body beneath the Colorado Plateau has peeled away from the crust, which has thinned rather than thickened, asthenosphere should have flowed up above into the region where dipping Moho reflectors are observed, generating a region of uplift in the central western Plateau during the last ~6 Ma (Levander *et al.* 2011). This broad region, extending from the Grand Canyon region and up towards the San Rafael Swell, has experienced 2–4 km of uplift during the last 30 Ma (Pederson *et al.* 2002b). Though most of the Grand Canyon uplift has been considered to have occurred in the last 6 Ma (Karlstrom *et al.* 2008; Crow *et al.* 2014), there has been recent debate, with arguments that Grand Canyon incision is instead related to subsidence at the eastern Plateau margin (Pederson

et al. 2002a) or uplift which initiated ∼50 Ma ago, about 200 km north-east of the Grand Canyon (Flowers *et al.* 2008).

As previously discussed, delamination beneath the Colorado Plateau may have stalled, in which case the lower crust could now have a cold steady-state geotherm, rather than the hot geotherm generated by active delamination, based on both our models (Fig. 9) and Valera *et al.* (2014). Our results predict that the surface above the instability switched to a state of subsidence when stalling occurred. This transition to subsidence does not occur in Valera *et al.* (2014), potentially as a result of buoyant granitic crust above the instability. Further modelling of the topographic evolution specific to the Colorado Plateau is therefore required to test the stalling hypothesis and to compare against the recent uplift evolution as it becomes clearer.

4.2 Sierra Nevada, California

The migration of restite from beneath the Sierra Nevada batholith, California, almost 100 km westward to its current location beneath the Great Valley (Saleeby *et al.* 2003), could be modelled by either triggered dripping or delamination. This ambiguity has implications for the recent focus on inferring rheological properties in this region from the observed timescales (Molnar & Jones 2004; Le Pourhiet *et al.* 2006). While the mechanism responsible for the initial instability growth is indistinguishable, any estimate of restite or decollement viscosity has at least an order of magnitude uncertainty. There are then two alternative interpretations of timescale data: either triggered dripping occurred with a high degree of rheological weakening, or delamination with a lesser degree of weakening.

The current morphology and stress-state of the instability and crust above is not necessarily indicative of how the instability initiated. For example, the temperature-dependent 2-D models demonstrate how easily an instability can begin by delamination and produce the corresponding observations, before switching to a dripping mode. For significant migration to occur, an initially planar step perturbation is most likely required. The extent of newly infiltrated asthenosphere below the Sierra Nevada, likely to correspond to the initial extent of the restite, is elongated parallel to the batholith and perpendicular to the direction of migration (Frassetto *et al.* 2011). This observation supports the hypothesis of an initially planar morphology, in which case the morphology has transitioned into a drip morphology.

The 3-D calculations demonstrate that a transition from a planar to drip morphology is not a natural progression of instabilities which are capable of migrating. Therefore if such a transition occurred beneath the Sierra Nevada, an additional process is required to trigger this switch. This may be a change in decollement conditions or interference with a competing dynamic process. For the former, the models predict that if the instability migrated into a region with a higher decollement viscosity, a step perturbation could transition into smaller wavelength instabilities with drip morphologies. Whether this transition occurs is dependent on the relative instability timescale compared to thermal diffusion. Models with a heterogeneous decollement are required for more detailed predictions. Alternatively, the finite length of the restite may have allowed 3-D curvature effects to interfere, a process which we have not modelled. Regardless of whether the instability began by triggered dripping or delamination, it is plausible that the instability has undergone some transition, which could provide further rheological inference if modelled in detail.

Inferring the type of initial mechanism from observed instability migration becomes ambiguous when considering the additional influence of background mantle flow. Our analysis assumes that the entire instability evolution is completely controlled by the mechanical properties and initial geometry of the lithosphere. However, the asthenosphere below the Sierra Nevada was inferred to be flowing at about 4 cm yr^{-1} in the same direction as migration of the instability (Zandt 2003) and the two may be coupled. If it is assumed that an instability has taken 10 Ma to double the lithosphere's thickness, its sinking velocity will still be at the cm yr^{-1} scale at this displacement and therefore could interact with mantle flow for its entire initial growth period. An instability would need to reach this displacement within ∼1 Ma in order for its initial growth to be isolated from surrounding flow. Though any instability will likely reach the 10 cm yr^{-1} scale during the rapid descent phase, the highest migration occurs during the initial phase in our models. It is therefore plausible that the migration of the Sierra Nevada drip is due to either asthenosphere flow, asymmetry in the initial instability conditions, or a combination of the two.

5 CONCLUSIONS

The mechanism by which dense lower continental crust and/or mantle lithosphere is recycled into the asthenosphere has a strong influence on the initial growth dynamics. Dripping, even if it is 'triggered', grows at an order of magnitude slower timescale than delamination. This is significant for lithosphere dynamics, considering that mass and energy flux, as well as the migration of surface expressions, follow this initial timescale. The triggering of delamination requires highly specific conditions: a weak decollement, intrusion of the asthenosphere into the lower crust and a timescale which can outpace thermal diffusion. Additionally, the instantaneous non-dimensional velocity of delamination when it is triggered is highly dependent on its coupling with the upper crust and this dependence can be accurately scaled by $L_c'^2/\eta_c'^{\frac{2}{3}}$. The acceleration which follows also scales accurately with the same dependence on η_c' and likely with L_c', though the latter was not explicitly modelled. Local tectonic processes and rheology control which mechanism occurs and therefore have a large impact on the dynamics of dense body recycling. This contrast in instability dynamics introduces uncertainty when inferring the viscosity and density of a sinking body if the instability mechanism is unclear. While dripping can be distinguished from delamination, triggered dripping produces similar characteristics to delamination and these would be difficult to discern in nature.

Using the simplistic model setup, the fundamental style of delamination growth has been characterized. It begins at a relatively high velocity which grows exponentially with time in two phases. The timescale of its initial growth depends on the viscosity of the sinking body. Delamination is likely to grow at a similar timescale to the thermal diffusion at the Moho. Sustained delamination may subsequently require an additional process to ensure that the weakness of both the decollement zone and in-flowing asthenosphere are maintained. A transition from planar to drip morphology, during the initial instability growth, is also likely to require an additional process. A switch to increased coupling between the crust and dense body, due to lateral rheological contrast, could trigger this transition.

Due to the variety in initial mechanism dynamics and later mechanism transitions, the dense lower crust and mantle lithosphere has the potential to be recycled in a number of contrasting ways. Rather than adding further ambiguity to the current debate of how

material is dominantly recycled beneath the continents, characterization of these mechanisms provides new constraints and models which observations of instability growth and morphology can be tested against, without assuming that one end-member mechanism always dominates over the other.

ACKNOWLEDGEMENTS

This research was supported by the Geological Survey of Western Australia (AB). It was undertaken with the assistance of resources from the National Computational Infrastructure (NCI), as well as the Pawsey Supercomputing Centre. These resources operate with funding from the Australian Government (NCI and Pawsey) and the Government of Western Australia (Pawsey). This research was also supported by ARC discovery grants DP1095166 and DP130101946 (LM) and the Marsden Fund VUW1407 (TS). We thank Oğuz Göğüş and an anonymous referee for their comments, which greatly contributed to an improved paper.

REFERENCES

Bajolet, F., Galeano, J., Funiciello, F., Moroni, M., Negredo, A.-M. & Faccenna, C., 2012. Continental delamination: insights from laboratory models, *Geochem. Geophys. Geosyst.,* **13,** Q02009, doi:10.1029/2011GC003896.

Bird, P., 1979. Continental delamination and the Colorado Plateau, *J. geophys. Res,* **84**(B13), 7561–7571.

Bird, P. & Baumgardner, J., 1981. Steady propagation of delamination events, *J. geophys. Res.,* **86**(B6), 4891–4903.

Burov, E. & Watts, A., 2006. The long-term strength of continental lithosphere: "Jelly sandwich" or "crème brûlée"?, *GSA Today,* **16**(1), 4–10.

Bystricky, M. & Mackwell, S., 2001. Creep of dry clinopyroxene aggregates, *J. geophys. Res.,* **106**(B7), 13 443–13 454.

Canright, D. & Morris, S., 1993. Buoyant instability of a viscous film over a passive fluid, *J. Fluid Mech.,* **255,** 349–372.

Capitanio, F., Morra, G. & Goes, S., 2007. Dynamic models of downgoing plate-buoyancy driven subduction: subduction motions and energy dissipation, *Earth planet. Sci. Lett.,* **262**(1), 284–297.

Chandrasekhar, S., 1961. *Hydrodynamic and Hydrostatic Stability,* Clarendon Press.

Conrad, C. & Molnar, P., 1999. Convective instability of a boundary layer with temperature-and strain-rate-dependent viscosity in terms of 'available buoyancy', *Geophys. J. Int.,* **139**(1), 51–68.

Conrad, C.P. & Molnar, P., 1997. The growth of Rayleigh–Taylor-type instabilities in the lithosphere for various rheological and density structures, *Geophys. J. Int.,* **129**(1), 95–112.

Crow, R., Karlstrom, K., Darling, A., Crossey, L., Polyak, V., Granger, D., Asmerom, Y. & Schmandt, B., 2014. Steady incision of Grand Canyon at the million year timeframe: a case for mantle-driven differential uplift, *Earth planet. Sci. Lett.,* **397,** 159–173.

Flowers, R., Wernicke, B. & Farley, K., 2008. Unroofing, incision, and uplift history of the southwestern Colorado Plateau from apatite (U-Th)/He thermochronometry, *Bull. geol. Soc. Am.,* **120**(5–6), 571–587.

Frassetto, A.M., Zandt, G., Gilbert, H., Owens, T.J. & Jones, C.H., 2011. Structure of the Sierra Nevada from receiver functions and implications for lithospheric foundering, *Geosphere,* **7**(4), 898–921.

Gilbert, H., Yang, Y., Forsyth, D., Jones, C., Owens, T., Zandt, G. & Stachnik, J., 2012. Imaging lithospheric foundering in the structure of the Sierra Nevada, *Geosphere,* **8**(6), 1310–1330.

Göğüş, O.H. & Pysklywec, R.N., 2008. Near-surface diagnostics of dripping or delaminating lithosphere, *J. geophys. Res.,* **113,** B11404, doi:10.1029/2007JB005123.

Gray, R. & Pysklywec, R.N., 2012. Geodynamic models of mature continental collision: evolution of an orogen from lithospheric subduction to continental retreat/delamination, *J. geophys. Res.,* **117,** B03408, doi:10.1029/2011JB008692.

Houseman, G.A. & Molnar, P., 1997. Gravitational (Rayleigh–Taylor) instability of a layer with non-linear viscosity and convective thinning of continental lithosphere, *Geophys. J. Int.,* **128**(1), 125–150.

Jones, C.H., Farmer, G.L. & Unruh, J., 2004. Tectonics of Pliocene removal of lithosphere of the Sierra Nevada, California, *Bull. geol. Soc. Am.,* **116**(11–12), 1408–1422.

Jones, C.H., Reeg, H., Zandt, G., Gilbert, H., Owens, T.J. & Stachnik, J., 2014. P-wave tomography of potential convective downwellings and their source regions, Sierra Nevada, California, *Geosphere,* **10**(3), 505–533.

Karlstrom, K.E., Crow, R., Crossey, L.J., Coblentz, D. & Van Wijk, J., 2008. Model for tectonically driven incision of the younger than 6 Ma Grand Canyon, *Geology,* **36**(11), 835–838.

Kaus, B.J. & Podladchikov, Y.Y., 2001. Forward and reverse modeling of the three-dimensional viscous Rayleigh–Taylor instability, *Geophys. Res. Lett.,* **28**(6), 1095–1098.

Kay, R.W. & Kay, S.M., 1993. Delamination and delamination magmatism, *Tectonophysics,* **219**(1–3), 177–189.

Krystopowicz, N.J. & Currie, C.A., 2013. Crustal eclogitization and lithosphere delamination in orogens, *Earth planet. Sci. Lett.,* **361,** 195–207.

Lamb, S., 2011. Cenozoic tectonic evolution of the New Zealand plate-boundary zone: a paleomagnetic perspective, *Tectonophysics,* **509**(3), 135–164.

Le Pourhiet, L., Gurnis, M. & Saleeby, J., 2006. Mantle instability beneath the Sierra Nevada mountains in California and Death Valley extension, *Earth planet. Sci. Lett.,* **251**(1), 104–119.

Lee, C.-T.A., Cheng, X. & Horodyskyj, U., 2006. The development and refinement of continental arcs by primary basaltic magmatism, garnet pyroxenite accumulation, basaltic recharge and delamination: insights from the Sierra Nevada, California, *Contrib. Mineral. Petrol.,* **151**(2), 222–242.

Lenardic, A. & Kaula, W., 1996. Near-surface thermal/chemical boundary layer convection at infinite Prandtl number: two-dimensional numerical experiments, *Geophys. J. Int.,* **126**(3), 689–711.

Levander, A., Schmandt, B., Miller, M., Liu, K., Karlstrom, K., Crow, R., Lee, C.-T. & Humphreys, E., 2011. Continuing Colorado plateau uplift by delamination-style convective lithospheric downwelling, *Nature,* **472**(7344), 461–465.

Lorinczi, P. & Houseman, G., 2009. Lithospheric gravitational instability beneath the southeast Carpathians, *Tectonophysics,* **474**(1), 322–336.

McEwan, A. & Taylor, G., 1966. The peeling of a flexible strip attached by a viscous adhesive, *J. Fluid Mech.,* **26**(01), 1–15.

Molnar, P. & Jones, C.H., 2004. A test of laboratory based rheological parameters of olivine from an analysis of late Cenozoic convective removal of mantle lithosphere beneath the Sierra Nevada, California, USA, *Geophys. J. Int.,* **156**(3), 555–564.

Molnar, P., England, P.C. & Jones, C.H., 2015. Mantle dynamics, isostasy, and the support of high terrain, *J. geophys. Res.,* **120**(3), 1932–1957.

Morency, C. & Doin, M.-P., 2004. Numerical simulations of the mantle lithosphere delamination, *J. geophys. Res.,* **109,** B03410, doi:10.1029/2003JB002414.

Moresi, L.-N. & Solomatov, V., 1995. Numerical investigation of 2D convection with extremely large viscosity variations, *Phys. Fluids,* **7**(9), 2154–2162.

Moresi, L., Muhlhaus, H. & Dufour, F., 2001. Particle-in-cell solutions for creeping viscous flows with internal interfaces, in *Bifurcation and Localisation Theory in Geomechanics*, pp. 345–354, eds Mühlhaus, H., Dyskin, A. & Pasternak, E., A.A. Balkema Publishers.

Moresi, L., Quenette, S., Lemiale, V., Meriaux, C., Appelbe, B. & Mühlhaus, H.-B., 2007. Computational approaches to studying non-linear dynamics of the crust and mantle, *Phys. Earth planet. Inter.,* **163**(1), 69–82.

Neil, E.A. & Houseman, G.A., 1999. Rayleigh–Taylor instability of the upper mantle and its role in intraplate orogeny, *Geophys. J. Int.,* **138**(1), 89–107.

Pederson, J., Karlstrom, K., Sharp, W. & McIntosh, W., 2002a. Differential incision of the Grand Canyon related to Quaternary faulting-Constraints from U-series and Ar/Ar dating, *Geology,* **30**(8), 739–742.

Pederson, J.L., Mackley, R.D. & Eddleman, J.L., 2002b. Colorado Plateau uplift and erosion evaluated using GIS, *GSA Today,* **12**(8), 4–10.

Poudjom Djomani, Y.H., O'Reilly, S.Y., Griffin, W. & Morgan, P., 2001. The density structure of subcontinental lithosphere through time, *Earth planet. Sci. Lett.,* **184**(3), 605–621.

Ribe, N.M., 1998. Spouting and planform selection in the Rayleigh–Taylor instability of miscible viscous fluids, *J. Fluid Mech.,* **377,** 27–45.

Ribe, N.M., 2010. Bending mechanics and mode selection in free subduction: a thin-sheet analysis, *Geophys. J. Int.,* **180**(2), 559–576.

Saleeby, J., Ducea, M. & Clemens-Knott, D., 2003. Production and loss of high-density batholithic root, southern Sierra Nevada, California, *Tectonics,* **22**(6), 1064, doi:10.1029/2002TC001374.

Sobolev, S.V. & Babeyko, A.Y., 2005. What drives orogeny in the Andes?, *Geology,* **33**(8), 617–620.

Stern, T., Houseman, G., Salmon, M. & Evans, L., 2013. Instability of a lithospheric step beneath western North Island, New Zealand, *Geology,* **41**(4), 423–426.

Turcotte, D.L. & Schubert, G., 2014. *Geodynamics,* Cambridge Univ. Press.

Valera, J., Negredo, A., Billen, M. & Jiménez-Munt, I., 2014. Lateral migration of a foundering high-density root: insights from numerical modeling applied to the southern Sierra Nevada, *Lithos,* **189,** 77–88.

Wang, H. & Currie, C.A., 2015. Magmatic expressions of continental lithosphere removal, *J. geophys. Res.,* **120**(10), 7239–7260.

Zandt, G., 2003. The southern Sierra Nevada drip and the mantle wind direction beneath the southwestern United States, *Int. Geol. Rev.,* **45**(3), 213–224.

Zandt, G., Gilbert, H., Owens, T.J., Ducea, M., Saleeby, J. & Jones, C.H., 2004. Active foundering of a continental arc root beneath the southern Sierra Nevada in California, *Nature,* **431**(7004), 41–46.